

An Accurate FEA of Turning Simulation and Parameters Optimization for Slender Shaft Turning

Tianlin Yang

A Thesis

In the Department

of

Mechanical, Industrial and Aerospace Engineering

Presented in Partial Fulfillment of the Requirements

For the Degree of

Master of Applied Science (Mechanical Engineering) at

Concordia University

Montreal, Quebec, Canada

July 2018

© Tianlin Yang, 2018

CONCORDIA UNIVERSITY
School of Graduate Studies

This is to certify that the thesis prepared

By: **Tianlin Yang**

Entitled: **An Accurate FEA of Turning Simulation and Parameters Optimization for Slender Shaft Turning**

and submitted in partial fulfillment of the requirements for the degree of

Master of Applied Science (Mechanical Engineering)

complies with the regulations of the University and meets the accepted standards with respect to originality and quality.

Signed by the final examining committee:

_____	Chair
Dr. Ming Yuan Chen	
_____	Examiner
Dr. Lin Lan	
_____	Examiner
Dr. Tsz Ho Kwok	
_____	Supervisor
Dr. Zezhong Chen	

Approved by _____

Dr. Mamoun Medraj, Chair of Department or Graduate Program Director

Dr. Amir Asif, Dean of Faculty of Engineering and Computer Science

Date _____

30/07/2018

ABSTRACT

An Accurate FEA of Turning Simulation and Parameters Optimization for Slender Shaft Turning

Tianlin Yang

There is a high demand to conduct high performance machining in industry to produce high quality parts with high efficiency. Thus, physical machining simulation is a must. Many researches have been conducted on machining simulation with the finite element analysis method. However, the prior machining simulation method is not completed, and the results are not reliable. In this thesis, a completed and accurate method of machining simulation is proposed. First, the cutting tool and the workpiece 3-D solid models are accurately built. These are often ignored in the prior methods. Second, the tool and the workpiece models are set up in the Thirdwave System machining simulation software according to the actual tool location and orientation in machining. Third, the adaptive meshing method is employed, and the mesh size is adapted for high accuracy and efficiency. Then, this approach is applied to a slender shaft turning. A detailed discussion on the constitutive equation for simulation is provided for more accurate results. The experiment results are used as a reference for the simulation model to improve the precision. Finally, the parameters for turning the slender shaft are optimized according to the simulated cutting temperatures and forces. The approach can be directly used in industry for high performance machining.

ACKNOWLEDGEMENTS

I hereby wish to express my sincerest gratitude and appreciation to my supervisor, Dr. Chevy Chen, for his priceless guidance and insights that lead me through this research. His meticulous attitude toward engineering research would keep on propelling me for the rest of my academic career. He is also a role model in my life, showing me how to be a responsible, dedicated and intelligent person. I would also like to thank my fellows in our lab for their generous support and ideas when I encountered problems. Finally, I give my special thanks to my parents for their unselfish love, my good friend, Zixi Fang, for his assistance in the past three years.

TABLE OF CONTENTS

LIST OF FIGURES	VII
LIST OF TABLES	XI
CHAPTER 1 INTRODUCTION	1
1.1 Background.....	1
1.2 Turning Tools.....	2
1.1.1 <i>Indexable Insert</i>	3
1.1.2 <i>Tool Holder</i>	3
1.3 Parametric Modeling.....	4
1.4 Literature Review	5
1.5 Problem Definition	8
1.6 Research Objective.....	10
1.7 Thesis Outline.....	10
CHAPTER 2 ACCURATE TURNING TOOL MODELING	11
2.1 Geometric Model of Physical Turning Simulation.....	11
2.2 Insert Solid Model	15
2.2.1 <i>Standard Insert Parameters</i>	15
2.2.2 <i>Insert Measurement and Modeling</i>	18
2.3 Measurement and Modeling of the Indexable Insert Tool Holders	36
2.3.1 <i>Geometry of Indexable Insert Tool Holders</i>	36
2.3.2 <i>Measurement of Insert Slot of Indexable Insert Tool Holder by Trilinear Coordinates</i> <i>Measuring Instrument</i>	40
2.3.3 <i>Indexable Insert Tool Holder Modeling</i>	41
CHAPTER 3 PHYSICAL TURNING SIMULATION WITH FINITE ELEMENT ANALYSIS.....	47
3.1 Introduction of Finite Element Analysis.....	47
3.2 Turning Simulation with AdvantEdge Software	48
3.2.1 <i>Instantaneous Workpiece Solid Model</i>	50
3.3 Workpiece Material.....	55
3.3.1 <i>GH4169 Performance and Machining Characteristics</i>	55

3.3.2 Constitutive Model for GH4169	57
3.4 Tool Material	62
3.4.1 Coating Material for Insert	62
3.5 Meshing in AdvantEdge.....	63
3.6 Tool Relocation.....	70
3.7 Finite Element Simulation Experiment Design.....	72
3.7.1 Selection of Cutting Parameters	73
3.7.2 Orthogonal Experimental Design	73
3.8 FEA Simulation by AdvantEdge	76
3.9 Advantages of the Optimal Simulation Method	79
CHAPTER 4 CUTTING PARAMETERS OPTIMIZATION.....	81
4.1 Introduction of Cutting Parameters Optimization	81
4.2 Analysis of S/N Ratio	81
4.3 Analysis of Variance	83
4.3 Verification	85
CHAPTER 5 CONCLUSIONS AND FUTURE WORK	88
5.1 Conclusions.....	88
5.2 Future Work	89
REFERENCES	90

LIST OF FIGURES

Figure 1.1 Turning tool.....	2
Figure 1.2 Indexable insert	3
Figure 1.3 Lathe tool holder.....	4
Figure 1.4 (a) AdvantEdge 2-D turning simulation, (b) AdvantEdge 3-D orthogonal simulation, (c) AdvantEdge real 3-D turning simulation	9
Figure 1.5 (a) AdvantEdge built-in turning models, (b) Accurate turning models.....	9
Figure 2.1 A 3-D geometric model of an insert cutting a workpiece in turning	12
Figure 2.2 Illustration of the orthogonal and the oblique cutting if turning with an insert.....	13
Figure 2.3 A simplified geometric model of the orthogonal cutting in turning	14
Figure 2.4 Basic turning insert parameters.....	16
Figure 2.5 A picture of a Korloy VBMT160408 insert and a Sandvik SVJBL 2525M16 tool holder	17
Figure 2.6 The Korloy® VBMT160408 insert is measured on an electric surface profiler	19
Figure 2.7 (a) VEBMT160408 PC9030 insert (b) An image plot of a rake face profile of the Korloy VBMT160408 insert	20
Figure 2.8 Retrieving the rake face data and the cutting-edge radius with the Digimizer software	21
Figure 2.9 A sketch of the rake face and cutting edge with the CATIA software	23
Figure 2.10 A 3-D solid model of the Korloy VBMT160408 insert	23

Figure 2.11 (a) An image plot of a rake face profile of the CCMT09T304MM insert, (b) Retrieving the rake face data and the cutting edge radius with the Digimizer software, (c) A sketch of the rake face and cutting edge with the CATIA software and (d) A 3-D solid model of the CCMT09T304MM insert 25

Figure 2.12 (a) An image plot of a rake face profile of the VBMT160404 insert, (b) Retrieving the rake face data and the cutting edge radius with the Digimizer software, (c) A sketch of the rake face and cutting edge with the CATIA software and (d) A 3-D solid model of the VBMT160404 insert..... 28

Figure 2.13 (a) An image plot of a rake face profile of the DNMG150608E-4E insert, (b) Retrieving the rake face data and the cutting edge radius with the Digimizer software, (c) A sketch of the rake face and cutting edge with the CATIA software and (d) A 3-D solid model of the DNMG150608E-4E insert..... 31

Figure 2.14 (a) An image plot of a rake face profile of the N123E2 0200 R0 1105 insert, (b) Retrieving the rake face data and the cutting edge radius with the Digimizer software, (c) A sketch of the rake face and cutting edge with the CATIA software and (d) A 3-D solid model of the N123E2 0200 R0 1105 insert..... 34

Figure 2.15 A picture of different indexable insert holders 36

Figure 2.16 A drawing of the SVJBL 2525M16 tool holder 38

Figure 2.17 Trilinear coordinates measuring instrument 40

Figure 2.18 3-D model of tool holder with insert shim..... 41

Figure 2.19 (a) A picture of a Korloy VBMT160408 insert and a Sandvik SVJBL 2525M16 tool holder, and (b) a 3-D solid model of the insert and the tool holder 42

Figure 2.20 (a) A picture of a CCMT09T304 Insert and a Sandvik A16M-SCLCL09 tool holder, and (b) a 3-D solid model of the insert and the tool holder	43
Figure 2.21 (a) A picture of a VBMT160404 Insert and a SVJBL3225 P16 tool holder, and (b) a 3- D solid model of the insert and the tool holder	44
Figure 2.22 (a) A picture of a Sandvik DNMG150608 Insert and a Sandvik DDJNR3225 tool holder, and (b) a 3-D solid model of the insert and the tool holder	45
Figure 2.23 (a) A picture of a Sandvik N123E2 Insert and a Sandvik RF123E15-2525B tool holder, and (b) a 3-D solid model of the Insert and the tool holder	46
Figure 3.1 The flow chart of using the Advantedge software for machining simulation	49
Figure 3.2 3-D models of the slender shaft turning components.....	50
Figure 3.3 Simulation of workpiece before machining.....	51
Figure 3.4 Simulation of No.1 tool turning the slender shaft.....	51
Figure 3.5 A section of the model of the raw workpiece before machining.....	52
Figure 3.6 The instantaneous workpiece model is generated by subtracting the envelop surface from the raw workpiece model.....	53
Figure 3.7 Parametric design of workpiece	54
Figure 3.8 Completed simplified workpiece	55
Figure 3.9 (a) User-defined JC constitutive model in AdventEdge (b) Usermath.dll.....	60
Figure 3.10 User-defined JC constitutive model simulation.....	61
Figure 3.11 Advantedge material simulation	61
Figure 3.12 Tool material	62
Figure 3.13 Tool coating.....	63

Figure 3.14 Tool meshing	64
Figure 3.15 CATIA to AdvantEdge	64
Figure 3.16 Simplified insert model	65
Figure 3.17 Relationship between mesh areas of insert and simulation result	66
Figure 3.18 Relationship between mesh precisions of insert.....	68
Figure 3.19 Mesh setting for workpiece	69
Figure 3.20 Sensitive test for workpiece mesh precision	70
Figure 3.21 (a) ISO Tool modeler (b) 3-D model of AdvantEdge built-in insert and workpiece	71
Figure 3.22 Turning orientation in AdvantEdge.....	72
Figure 3.23 (a) Telecom 360 postprocessor, (b) Cutting edge temperature distribution	77
Figure 3.24 (a) Simulation of chip deformation, (b) Chip deformation after one revolution	78
Figure 3.25 (a) Simulation with built-in 3-D model and mesh setting, (b) Simulation with accurate 3-D model and optimized mesh setting	80
Figure 3.26 Simulation time screenshot from AdvantEdge workbench.....	80
Figure 4.1 S/N response graph for force X.....	82
Figure 4.2 (a) No.3 experiment (b)No.1 experiment (c) Optimized experiment.....	86

LIST OF TABLES

Table 2-1 The model list of the tools used in turning a slender shaft	15
Table 2-2 Parameters of the Korloy® VBMT160408 insert	17
Table 2-3 The parameters of the VBMT160408 insert.....	22
Table 2-4 The parameters of the CCMT09T304MM insert.....	26
Table 2-5 The parameters of the VBMT160404 insert.....	29
Table 2-6 The parameters of the DNMG150608E-4E insert	32
Table 2-7 The parameters of the N123E2 0200 R0 1105 insert.....	35
Table 2-8 Parameters of the example indexable insert tool holder SVJBL 2525M16	39
Table 3-1 Thermal conductivity and specific heat properties of high-temperature alloy GH4169	56
Table 3-2 Linear expansion coefficient of high-temperature alloy GH4169	56
Table 3-3 The mechanical properties of GH4169.....	56
Table 3-4 Johnson-Cook material model designation of material constants.....	58
Table 3-5 Parameters of JC constitutive equation for GH4169.....	58
Table 3-6 Parameters of JC constitutive equation for GH4169.....	65
Table 3-7 Sensitive rate test for tool mesh precision.....	67
Table 3-8 Cutting parameters and their levels.....	74
Table 3-9 L9 orthogonal array	75
Table 3-10 Experiment array for FEA simulation.....	76

Table 3-11 Simulation and meshing time comparison.....	80
Table 4-1 S/N ratio for minimize force X.....	82
Table 4-2 F-table for $\alpha=0.05$	83
Table 4-3 Analysis of variance for force X.....	84
Table 4-4 Optimized cutting parameters simulation result	85

CHAPTER 1 INTRODUCTION

1.1 Background

In the manufacturing industry, it is quite challenging to turn slender shafts with high precision and efficiency. Shafts are essential in aero-engines, automobiles and machine tools, which require high accuracy and surface finish. Among the shafts, there are some slender shafts, which are defined as having a ratio of length and diameter that is greater than 15. Due to the high length-diameter ratio, during the cutting process, the shaft often produces a bending deformation. Therefore, the turning of slender shafts is a challenge for the industry.

The material of the aircraft slender shafts is nickel-based superalloy. Its physical and mechanical properties include high shear strength, low thermal conductivity, work-hardening tendency, highly abrasive carbide particles, strong tendency to weld and to form a built-up edge [1]. Thus, it is challenging to cut, and the aircraft slender shaft is expensive due to the high price of the material and high machining cost. Most recently, to turn superalloy material, people are using the carbide and ceramic tools because they have very high hardness and wear resistance [2-4]. To establish a reliable slender shaft manufacturing process, numerous cutting experiments are usually conducted to determine proper cutting tools and machining parameters. Therefore, cutting process simulation could save cost and time compared with the traditional way. Recently, the finite element method (FEM) has been developed as an efficient and convenient tool for cutting process simulation in order to obtain the required forces and the temperatures [6-16].

This thesis describes an application of the finite element method simulation for slender shaft turning. The method helps to improve the tool process parameters, to extract the cutting-edge data during the turning process, and to optimize shaft surface finish or toolpath at a proper position.

1.2 Turning Tools

Turning tools play a fundamental role in machining cutters and are widely used in the axial parts of the manufacturing industry. Today, with the rapid development of manufacturing, the solid turning tool has been replaced by the indexable tool, which is much more cost-effective because the cutter head can be replaced. A modern turning tool has two significant parts: Indexable insert and Tool holder. Currently, several categories of turning tools exist in the industry such as threading, boring, grooving, front turning and back turning as shown in Figure 1.1. They can be divided by the rake angle of the insert, by the function of the tool, by lead angle of the tool and by material.

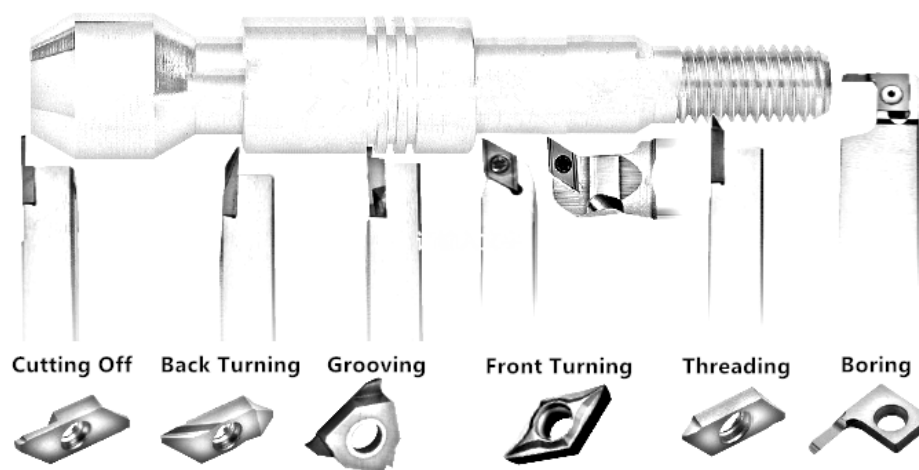


Figure 1.1 Turning tool

1.1.1 Indexable Insert

Indexable inserts are removable cutting tips. They are indexable and not welded with the tool holder, meaning that they can be exchanged with many types, and can also often be rotated or flipped. Different turning processes can change different inserts to ensure the best performance. An insert always has a coating on its outside surface to improve cutting properties and to extend its life. A turning indexable insert is shown in Figure 1.2. The slot on the rake face of the turning tool is used to break the metal chip, with a radius at the corner which can extend tool life. And the hole on the central part is used to fix the indexable insert on the tool holder.

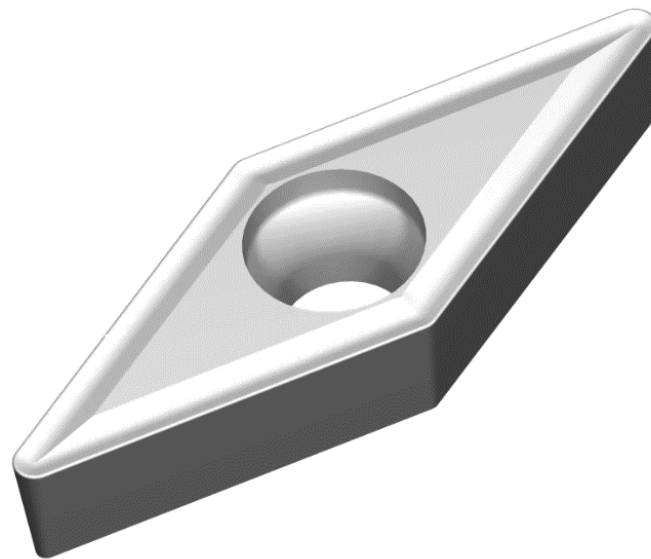


Figure 1.2 Indexable insert

1.1.2 Tool Holder

The tool holder is a support for the insert. It can be fixed on a lathe tool adapter. Each insert has its specialized holders. Different holders can offer different lead angle, rake angle, and relief angle for the installed insert. There are many methods for holding the insert like top

clamping, top and hole clamping, and screw clamping through the hole. And many ISO standard types of tool holder are being widely used in the industry [30]. A standard lathe tool holder is shown in Figure 1.3.

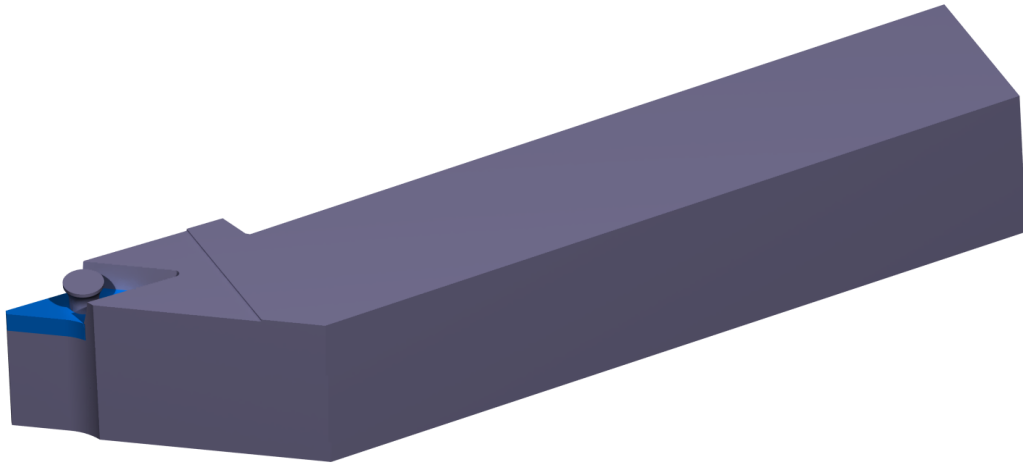


Figure 1.3 Lathe tool holder

1.3 Parametric Modeling

In Computer Aided Design (CAD), the parametric modeling techniques play a mean role for batch modeling. It can easily build or modify design by changing the values of the parameters. The basic of Parametric Modeling is using parameters to represent geometric features, and to connect dimensions with equations and numbers. Compared with the traditional modeling method, the parametric modeling method clearly defines relations between dimensions and constraints. It can save time and avoid manual work errors.

To fulfill the special requirements of the lathe tool parametric modeling, a commercial CAD software such as Catia is required. The tool model with parameters can be written with custom rules and transferred into an FEA software and be used to calculate. Then, by changing turning

parameters, such as cutting depth, feed rate, and diameter of the workpiece, the software will be automatically generating a suitable 3-D model of lathe tool for FEA calculation.

1.4 Literature Review

Metal cutting parameter optimization has been researched for many years. Studies have been conducted to prove that the surface roughness of the turning process can be improved by changing the tool chamfer angle and cutting parameters [3]. In 1971, Weinmann and Turkovich [4] studied the chip deformation in the orthogonal turning of 70/30 brass. Their research provided experimental cutting forces and shear information with different rake angles of tools. In 1984, Usui, Shirakashi and Kitagawa [5] presented an analytical method for carbide turning tool wear prediction. Today, it is still used for determining tool wear and tool life in FEA softwares such as AdvantEdge. In 2004, Joshi [6] used AdvantEdge 2-D simulation to find that chip segmentation can't be observed when tools are at positive rake angles. In 2005, Ahmed, et al. [7] developed a 3-D model of UAT to analyze the influence of tool geometry on cutting parameters, and to predict chip formation by FEA simulation. Li and Shih [8], using AdvantEdge, did a 3-D orthogonal turning simulation for titanium. They used AdvantEdge for a study on chip curl and chip flow direction. In 2007, Zhou, Yip-Hoi and Huang [9] found the Tool-Workpiece Engagement (TWE) geometry for turning. The research provided an efficient geometry for turning process modeling and optimization, which can be used for FEA. Pawade, et al. [10] investigated the cutting forces and surface damage in high speed turning of Inconel 718, and found the effects of tool edge geometry and machining parameters on cutting forces and surface finish. They used the ANOVA approach and they found out that the best parameters for the minimum force were

cutting speed 475 m/min with 0.1 mm/rev feed rate and depth of cut 0.5 mm when turning with a 30° chamfered and honed insert. Uhlmann and Graf [11] compared turning process simulated forces with experimental forces by ABAQUS 3-D ABAQUS 2-D and DEFORM 2-D, and discovered that the tool chamfer will cause problems to 3-D FEA cutting process simulations. In 2011, Ozel, et al. [12] compared 3-D machining models between DEFORM 3-D and ABAQUS. They used the Johnson-Cook material model for Inconel 718. The results show that FEA simulation gets larger forces than a real experiment, and that the DEFORM-3-D approach is better than ABAQUS for predicting cutting forces. In 2014, Jafarian and Imaz [13] conducted a study on JC material constants. They found the material model directly changes FE simulation results, and that some parameters can improve the accuracy of the simulation including damage value (D), global heat transfer coefficient (h), and frictional constants (m and μ). Mitrofanov, Babitsky and Silberschmidt [14] used the finite element method for ultrasonically assisted turning (UAT). They found that the residual strains is 20% lower in simulation compared with UAT. In 2015, Yadav, Abhishek and Mahapatra [15] used DEFORM 3-D simulation which allowed them to predict the tool wear and the material removal rate (MRR) in turning of Inconel 718. This was verified with experimental data. They found that the error margin between simulation and experiment is below 7%. In 2018, Zhang and Ding [16] provided a hybrid digital image correlation (DIC) finite element modeling approach for orthogonal cutting modeling. The DIC technique is used to study the deformation of the workpiece. This approach could directly use images for FEA simulation and for generating geometries of tool-chip interface. They found that the simulated tangential cutting forces were similar to experimental data.

About the optimization of turning, Tang, Landers and Balakrishnan [17] used a novel heuristic approach to optimize cutting parameters for parallel turning. The minimum machining time is the optimization target. Zkeri, Rech and Altan [18] used FEA for dry turning optimization in 2009. The effect of edge hone radius on insert temperature and stress was found to optimize further insert geometry. Chomsamutr and Jongprasithporn [19] used the Taguchi method. It improved the product quality of turning operations. The optimized cutting parameter verified with surface roughness, straightness and roundness indicated that feed rate is the most critical parameter for turning surface quality. The researchers got 0.15mm straightness and 0.15mm roughness improvements in 2010. In 2012, Prete and Vitis [20] studied the turning tool engage for Inconel 718. They found that when the tool engagement angle is 45° with high depth of cut values, the tool breakage will occur with high probability. Zhang, Li and Wang [21] compared tool life and cutting forces in milling Inconel 718 between dry machining and cooling lubrication machining. Under a minimum quantity cooling lubrication cutting condition, the cutting forces dramatically decrease. And the tool life is 1.57 times longer than in a dry cutting condition. In 2013, Camposeco-Negrete, Calderón-Nájera and Miranda-Valenzuela [22] used the robust design technique to optimize the power consumption during turning. This was successful because they optimized cutting parameters to minimize power consumption. Yildiz [23] optimized the cutting parameters in multi-pass turning by using the artificial bee colony-based approach. He used function evaluations 4000 to get solutions that were much better than the traditional GA algorithm. Vijay and Krishnaraj [24] used Taguchi and ANOVA methods for end milling Ti-6-Al-4V cutting parameters optimization. They found that the feed rate had the most effect on surface roughness. In 2016, Wang, et al. [25] used the neural network and genetic algorithm optimized

high-speed milling cutting parameters. After the research, they got multi optimized parameters. They then used these parameters to improve efficiency and machining quality. In 2017, Satyanarayana, Reddy and Nitin [26] used DEFORM 3-D and created an FEA model for high speed dry turning of Inconel 718 and they optimized the parameters using ANOVA and GA. They indicated that the cutting speed did the most contribution on insert flank wear and temperature during the machining. Li, Tang et al. [27] presented an approach for energy aware CNC machining cutting parameter optimization. The multi-objective annealing algorithm has been used for process planning and optimization. The best achieved is 31% energy consumption reduction.

1.5 Problem Definition

In this research, the Thirdwave System AdvantEdge has been used for turning simulation. It is an industry-approved FEA simulation software dedicated for machining. And it provides 2-D turning as shown in Figure 1.4(a), 3-D Orthogonal turning as shown in Figure 1.4(b) and real 3-D turning models as shown in Figure 1.4(c). For turning simulation, most studies do not use a real 3-D simulation model. The 2-D turning model and 3-D orthogonal turning model are widely used because they are easier for simulation. They can't represent turning processes with the lead angle and insert geometries. Because of this, the results had lower accuracy, compared to the results of the real 3-D model. In AdvantEdge, compared with accurate turning model demonstrated in Figure 1.5(b), the built-in turning models illustrated in Figure 1.5(a) are inaccurate. The simulation settings must be customized for each toolpath of turning process. Therefore, to analyze turning process instantaneously, the problems to be solved in this research are:

- To replace inaccurate built-in turning models in AdvantEdge, real insert and tool holder models should be provided to improve simulation accuracy.
- To analyze the slender shaft turning process instantaneously, the instantaneous workpiece model for simulation should be established.
- In order to save time and improve the accuracy of the experiment, simulation settings need to be customized for the real 3-D model of slender shaft turning.
- To utilize experiment results, optimized cutting parameters should be found.

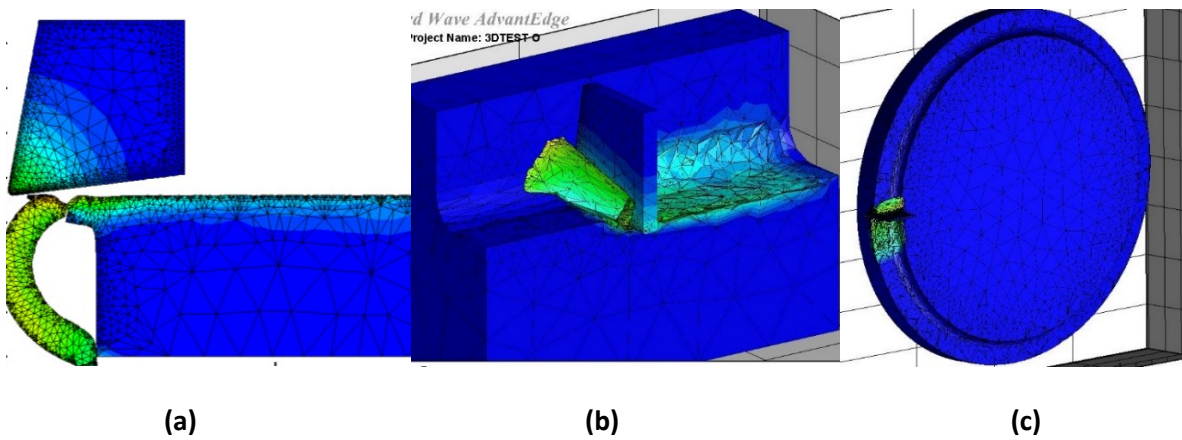


Figure 1.4 (a) AdvantEdge 2-D turning simulation, (b) AdvantEdge 3-D orthogonal simulation, (c) AdvantEdge real 3-D turning simulation

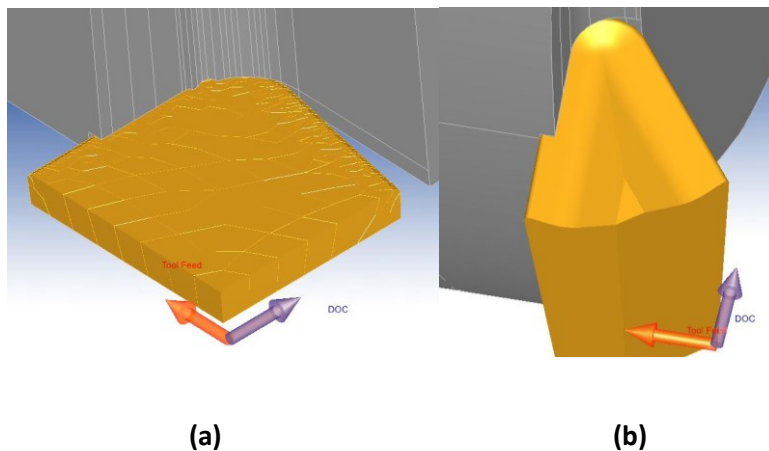


Figure 1.5 (a) AdvantEdge built-in turning models, (b) Accurate turning models

1.6 Research Objective

The objectives of this thesis focus on proposing a method of lathe cutting simulation and turning parameters optimization. The work can be concluded by the following aspects:

- Accurate lathe machining tool and workpiece modeling.
- The actual cutting position of tools and meshing in Thirdwave AdvantEdge software.
- Accurate FEA simulation of the lathe cutting.
- Cutting parameters optimization by Taguchi method and analysis of variance (ANOVA).

1.7 Thesis Outline

This thesis consists of 5 chapters. CHAPTER 1 gives a general introduction about the turning FEA simulation system. CHAPTER 2 explains the lathe tools modeling. CHAPTER 3 describes the slender shaft workpiece parametric design and the machining simulation optimization. CHAPTER 4 shows the cutting parameter optimizations. CHAPTER 5 concludes the work of the FEA simulation system and proposes the possible future work.

CHAPTER 2 ACCURATE TURNING TOOL MODELING

2.1 Geometric Model of Physical Turning Simulation

Turning operation is a major method of cutting cylindrical workpieces, and it takes about 25% of the metal removing job. To cut different features, such as cylinders with a shoulder on the left and right side, slots and end faces, turning tools are different in shape. To cut different workpiece materials, the tools are different in parameters. To predict cutting force, cutting temperature and tool wear in the physical simulation of turning, the geometric details of an insert turning a workpiece is investigated. In Figure 2.1(a), the insert is cutting a workpiece, the insert is fixed and the workpiece is rotating along the lathe axis. It clearly shows how the insert side cutting edge engages with the workpiece at a moment. To highlight the geometric detail of this cut, a point on the side cutting edge is sampled. At this point, the tangent of the side cutting edge is found, and the cutting speed direction is normal to the radius line of the point. Then, a plane normal to the tangent is passing through the cutting intersects with the insert and the workpiece, and the sectional view is plotted in Figure 2.1(b). In this figure, the insert top surface near the cutting edge is the rake face. The angle between the rake face and the normal to the cutting speed is the rake angle. Generally, a rake angle can be negative or positive depending on the workpiece and the insert materials. In roughing, inserts with negative rake angles are often used for greater cutting force and higher cutting temperature. In finishing, inserts with positive rake angles are used for less cutting forces and better surface roughness. The insert surface close to (or contacting) the machined surface is the relief or the flank face. The clearance angle is the

angle between a workpiece line and the flank. If the clearance angle is small, the flank could rub the machined surface, causing flank wear and reducing the machined surface finish. If the clearance is large, the insert cutting edge is less strong.

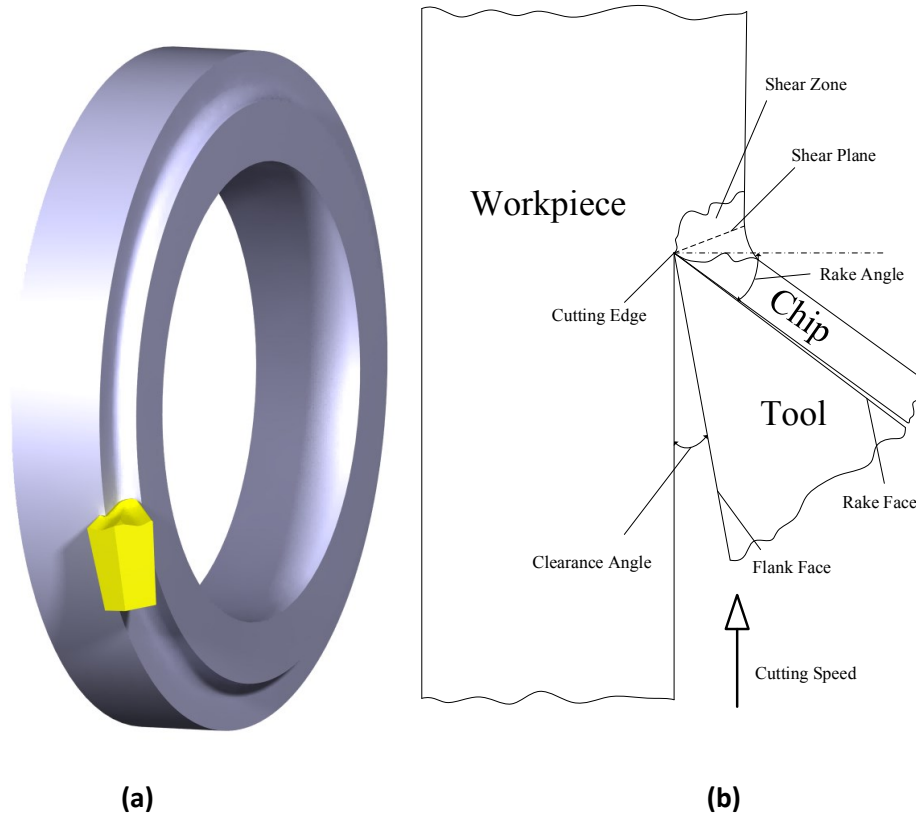


Figure 2.1 A 3-D geometric model of an insert cutting a workpiece in turning

In terms of the relationship between the cutting speed direction and the insert cutting edge, the cutting mechanism is distinguished with orthogonal and oblique cutting. (see Figure 2.2). The orthogonal and oblique cutting is illustrated in Figure 2.2 and explained in the following.

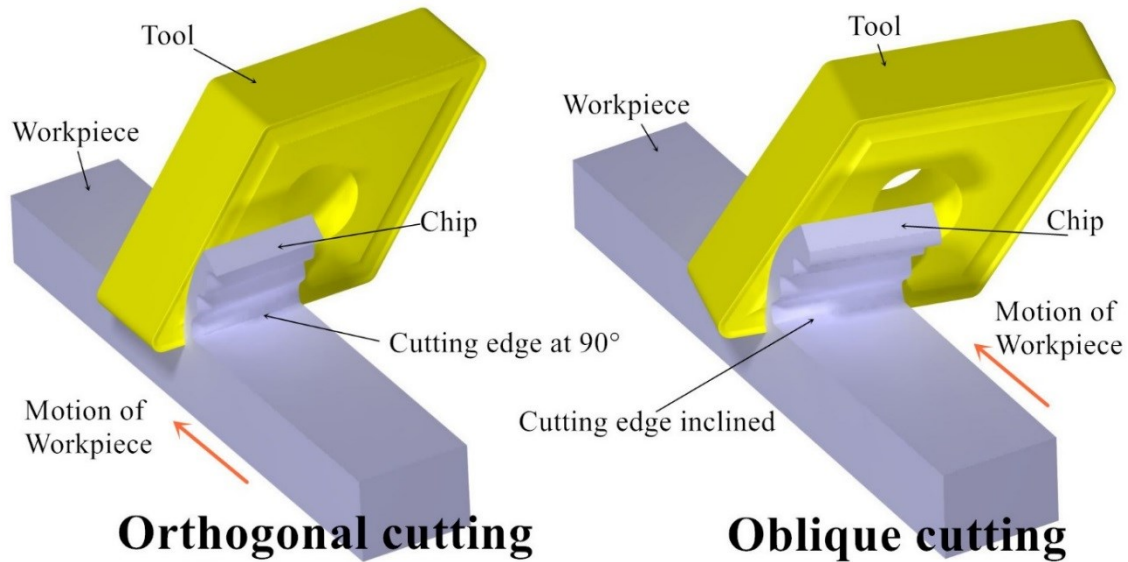


Figure 2.2 Illustration of the orthogonal and the oblique cutting if turning with an insert

In turning, an insert tool cuts a workpiece, which rotates along the main axis of the lathe. If the side cutting edge of the insert is perpendicular to the cutting speed direction, it is the orthogonal cutting. If the side cutting edge of the insert is not perpendicular to the cutting speed direction, it is the oblique cutting. To conduct physical simulation for turning, the geometry of the insert cutting the workpiece should be simplified by only focusing on the neighbor of the insert and the workpiece at their engagement. Figure 2.3 shows the simplified geometric model of an orthogonal cutting simulation, and the terms used in the model are labeled.

the cutting forces will dramatically decrease

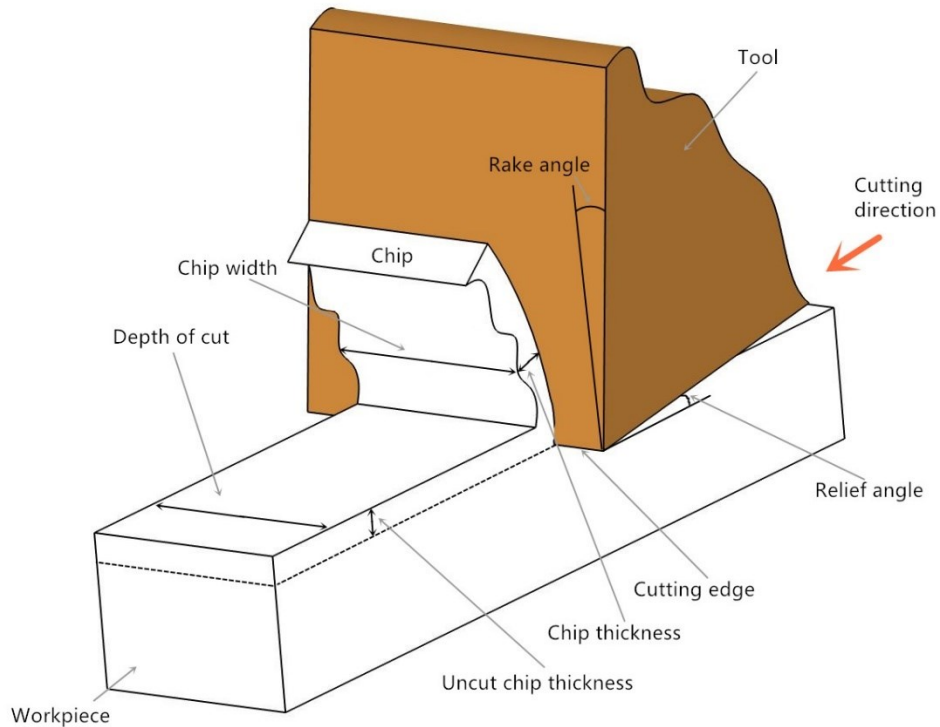


Figure 2.3 A simplified geometric model of the orthogonal cutting in turning

Most studies do not use real 3-D simulation. The accuracy of the tool and workpiece model are often neglected. In this research, the accurate real 3-D geometric model as shown in Figure 2.1(a) has been generated. The real 3-D geometric model contains insert chip breaker, insert rounded corner and instantaneous workpiece models. Compared with the simplified geometric model, it can represent the real working position of the turning tool in FEA system, and simulate the turning process as close to reality as possible. The method to establish the accurate 3-D model will be explained in this chapter.

2.2 Insert Solid Model

It is important to build genuine 3-D solid models with CAD software for inserts used in turning. The rake face, the cutting-edge radius, and the flank are critical to physical simulation. In turning a slender shaft, five tools and tool holders are used, whose models are listed in Table 2-1.

Table 2-1 The model list of the tools used in turning a slender shaft

No.	Insert	Tool holder
1	VBMT160408 PC9030	SVJBL 2525M16
2	CCMT09T304MM 1105	A16M-SCLCL09
3	VBMT160404 PC9030	SVJBL3225 P16
4	DNMG150608E-4E	DDJNR3225 P15
5	N123E2 0200 R0 1105	RF123E15-2525B

2.2.1 Standard Insert Parameters

A turning tool includes an insert and a tool holder. Usually, the 3-D solid models of turning tools are not provided by manufacturers. To conduct machining simulation with high fidelity, the turning tool should be modeled with the same shape as the actual tool shape. For this purpose, the specifications of the insert and the tool holder parameters should be obtained according to the ISO and the company standards. Inserts are classified into different groups for roughing, semi-finishing and finishing. They are classified for external and internal turning.

Figure 2.4 shows the basic turning insert parameters. Angle α is the angle between two cutting edges, it is the smaller angle of interior corners. Angle α_c is the normal clearance angle. The edge length l is the distance between two equilateral points of insert rhombus. Insert

thickness s is measured from its top face to its bottom face. Radius r is the insert corner radius, which determines the workpiece surface finish. The larger the insert radius, the better the surface roughness of the part. But if the radius is oversized, due to the insert-workpiece contact area increasing dramatically, the tool can vibrate in machining. Parameter d is the nominal diameter of the insert inscribed circle. Parameter d_1 is the diameter of the insert's central hole. Parameters m_1 and m_2 are the largest distance between the inscribed circle and the insert corner. The chip breakers on insert rake face are indicated in the section view as two curves relies on the left side. It's a slot shoulder in a turning insert made by grinding a groove parallel to the cutting edge. During cutting, a continuous chip flows over the chip breaker. It is easily broken into pieces and is removed. In this work, a Korloy® insert with the model of VBMT160408 is used and shown in Figure 2.5. The parameter values of the insert are given and listed in Table 2-2.

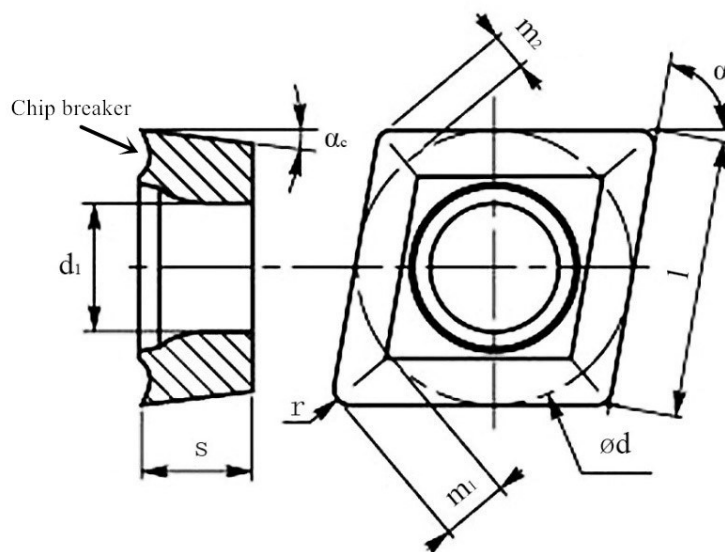


Figure 2.4 Basic turning insert parameters



Figure 2.5 A picture of a Korloy VBMT160408 insert and a Sandvik SVJBL 2525M16 tool holder

Table 2-2 Parameters of the Korloy® VBMT160408 insert

Parameters	Definition	Value
α	Included angle	35°
α_c	Normal clearance angle	5°
l	Edge length	16.606 mm
s	Insert thickness	4.762 mm
r	Radius of insert rounded corner	0.794 mm
d	Diameter of the inscribed circle of the insert	9.525 mm
d_1	Inner diameter of blade round hole	4.4 mm
m_1	Distance between the diameter of inscribed circle and the insert rounded corner	9.229 mm
m_2		0.193 mm

2.2.2 Insert Measurement and Modeling

Although some insert parameter specifications can be found from the aforementioned, the important information about the inserts, such as the cutting-edge radius, the rake angle and the chip breaker geometry are trade secrets, the information cannot be found. In this work, an electric surface profiler with a model of CONTOURECORD 600D is used to measure the insert geometry for the insert profile point coordinates. A picture of this instrument is displayed in Figure 2.6. To measure the insert, first, the insert is setup on the instrument; second, the insert coordinate system is built. Then, a needle-type stylus slides on the insert surface to measure points on many profiles, and the profile point coordinates are stored. The accuracy of this instrument is 0.1 micro, so the measured point coordinates are very accurate. This instrument has been used in a cutting tool company for production, it is reliable. Since the needle-type stylus is quite sharp at the end, it can access the insert surface points even though the surface geometry is complex, as shown by the cutting-edge, the rake face and the chip breaker. Unfortunately, the measured surface can be scratched by the stylus. With this instrument, the cutting-edge radius, the rake angle and the chip breaker geometry can be measured accurately.

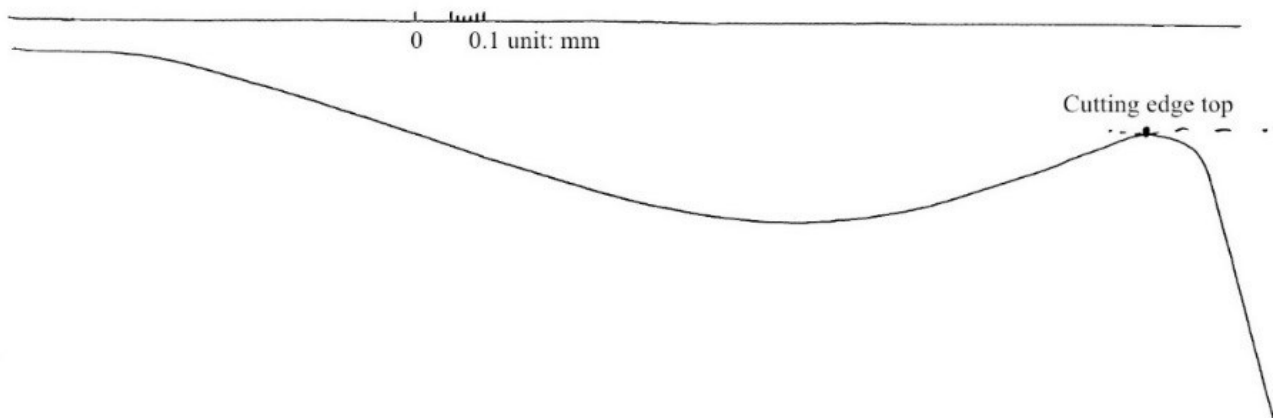


Figure 2.6 The Korloy® VBMT160408 insert is measured on an electric surface profiler

The cutting edge radius and the rake angle of the Korloy® VBMT160408 PC9030 insert shown in Figure 2.7(a) are the most important parameters to cutting force, tool temperature, and tool life. The profile crossing the rake face, the cutting edge and the flank face are measured and are plotted in Figure 2.7(b). The plot image is printed by profiler with 1:100 throw Ratio. It is measured by a stylus crossing the vertical direction of the cutting edge.



(a)

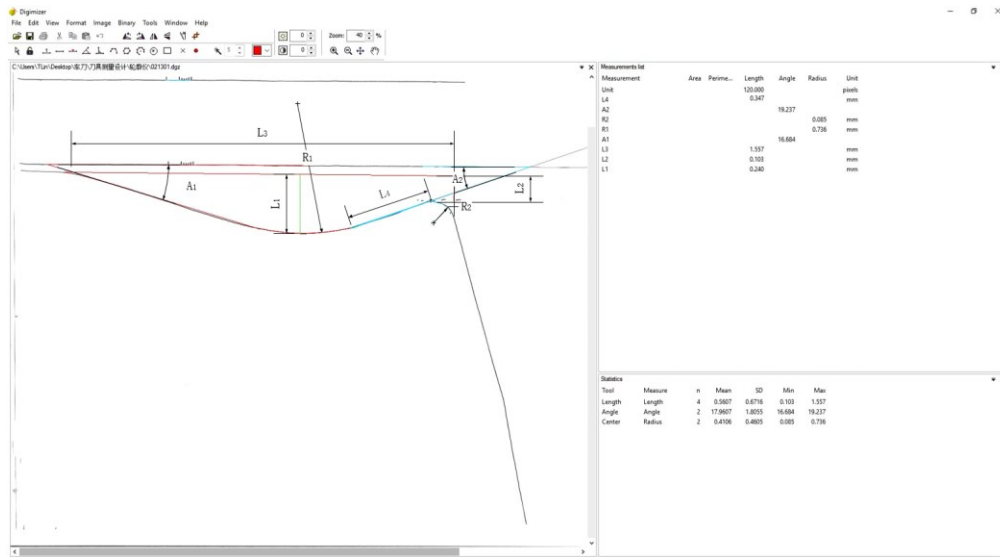


(b)

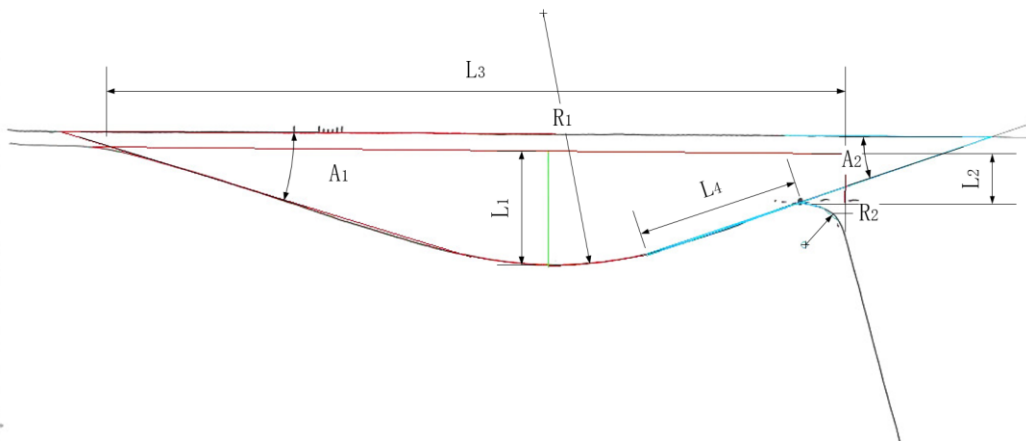
Figure 2.7 (a) VEBMT160408 PC9030 insert (b) An image plot of a rake face profile of the Korloy VBMT160408 insert

Because of the contour lines provided, the mapping instrument cannot directly provide the dimension information. An image processing technique is needed to measure the original image. Compared with the manual measure method, the computer image software will provide more

reliable measurements. In order to measure the angle length and calibrate the pixel size more conveniently and accurately, the Digimazer® software is used for image processing and analysis. Figure 2.8 shows the detected VBMT160408 insert rake face contour line with the basic sizes and angles. Table 2-3 lists the parameters for VBMT160408 insert.



(a)



(b)

Figure 2.8 Retrieving the rake face data and the cutting-edge radius with the Digimazer software

Table 2-3 The parameters of the VBMT160408 insert

Parameters	Definition	Value
L_1	Maximum vertical distance between chip breaker curve with insert rake face	0.24 mm
L_2	Vertical distance between cutting edge corner initial point with insert rake face	0.103 mm
L_3	Horizontal length for cutting edge profile	1.557 mm
L_4	Cutting edge rake face length	0.347 mm
A_1	Angle between horizontal reference plane with the joint line for insert rake face	16.684°
A_2	Cutting edge rake angle	19.237°
R_1	Radius of chip breaker slot	0.736 mm
R_2	Cutting edge radius	0.085 mm

Following the ISO 3364 standard [31], a rake face contour model is established according to the mentioned dimensions. Figure 2.9 shows the rake face contour CAD model in commercial software CATIA®.

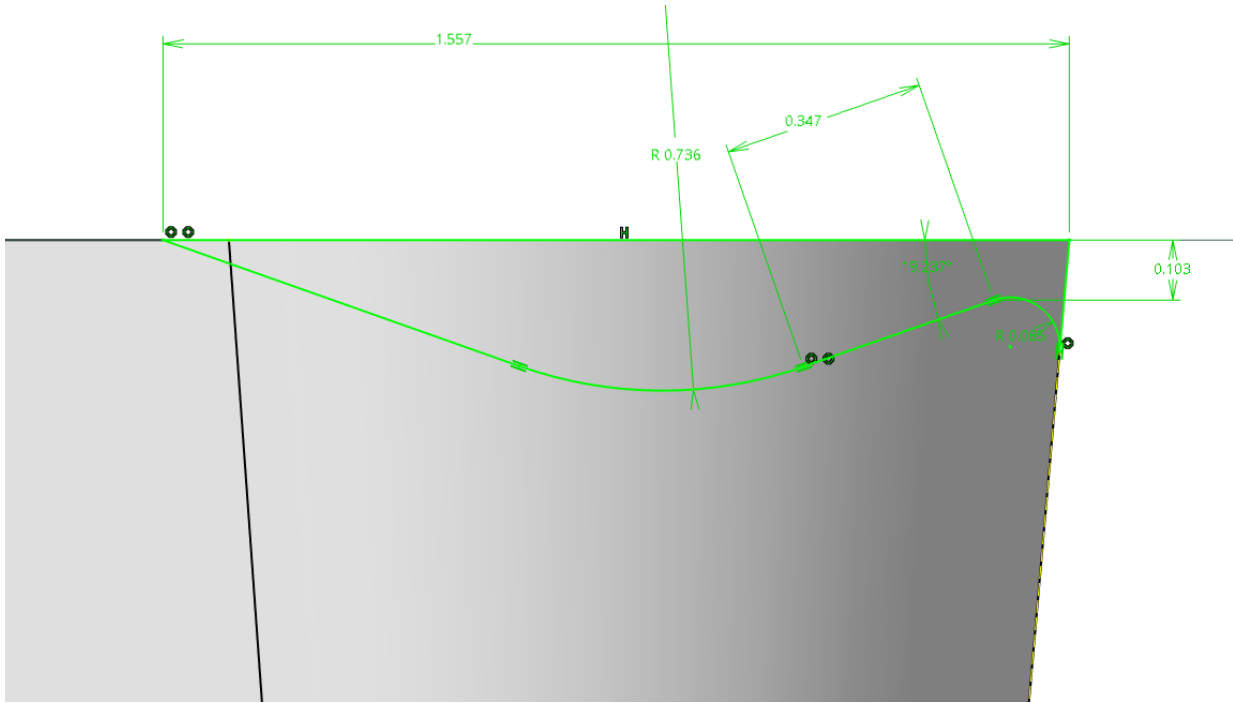


Figure 2.9 A sketch of the rake face and cutting edge with the CATIA software

After obtaining the rake angle and the cutting-edge radius, together with the previously obtained insert parameter values, an accurate 3-D model of the Korloy VBMT160408 insert is generated with the CATIA® CAD/CAM software. This model is shown in Figure 2.10.

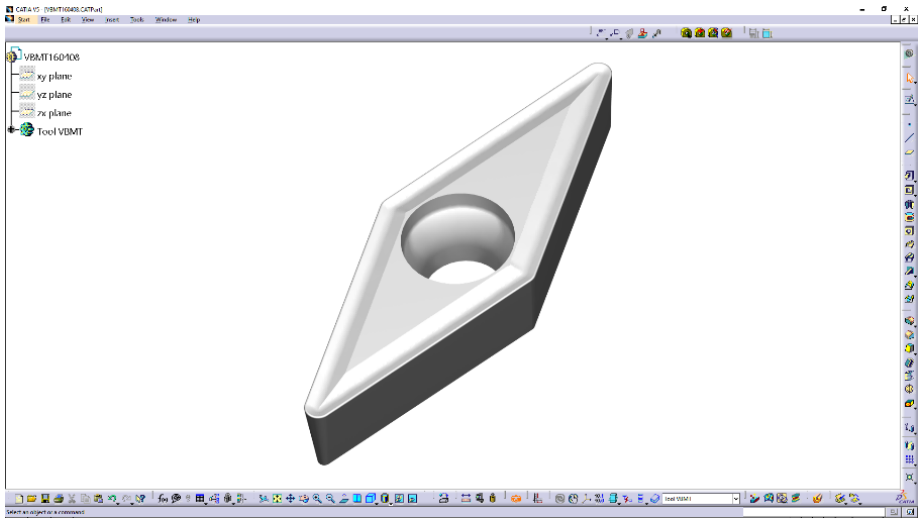
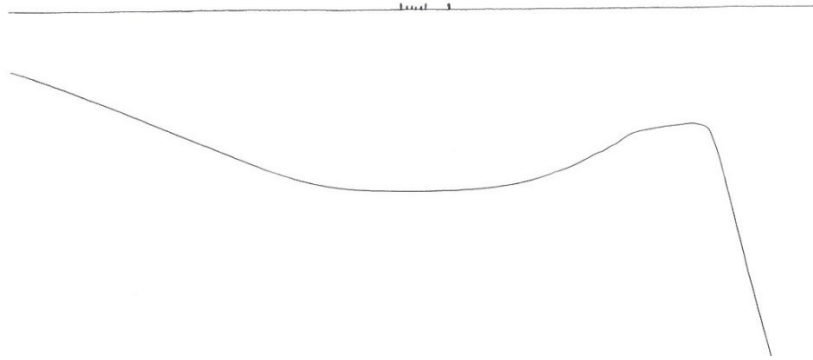
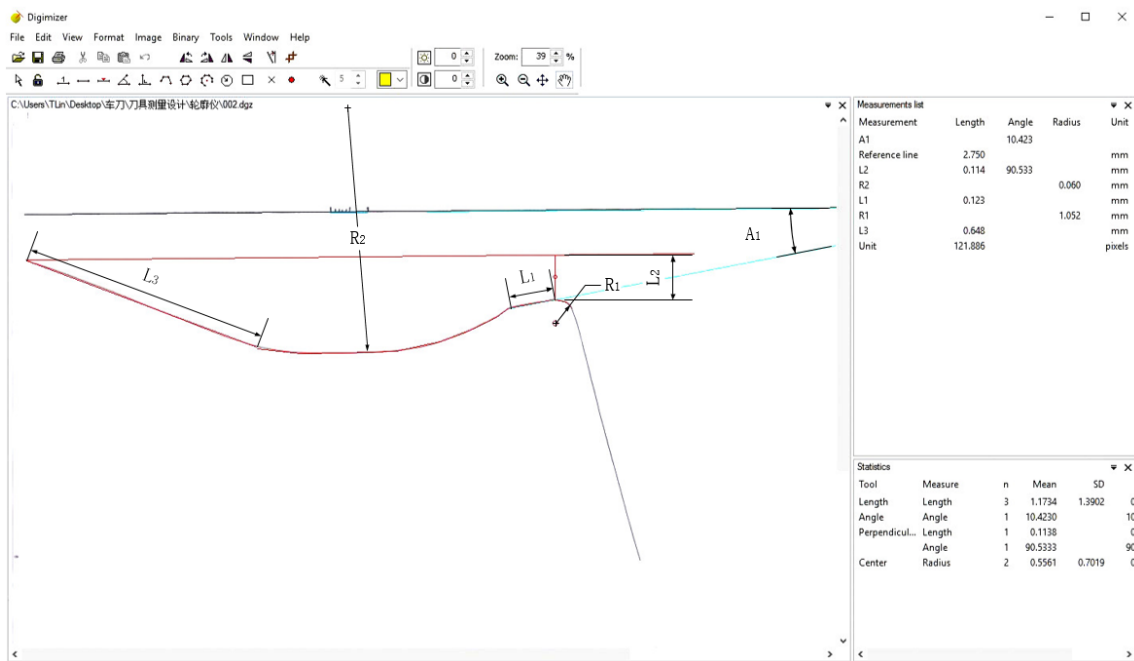


Figure 2.10 A 3-D solid model of the Korloy VBMT160408 insert

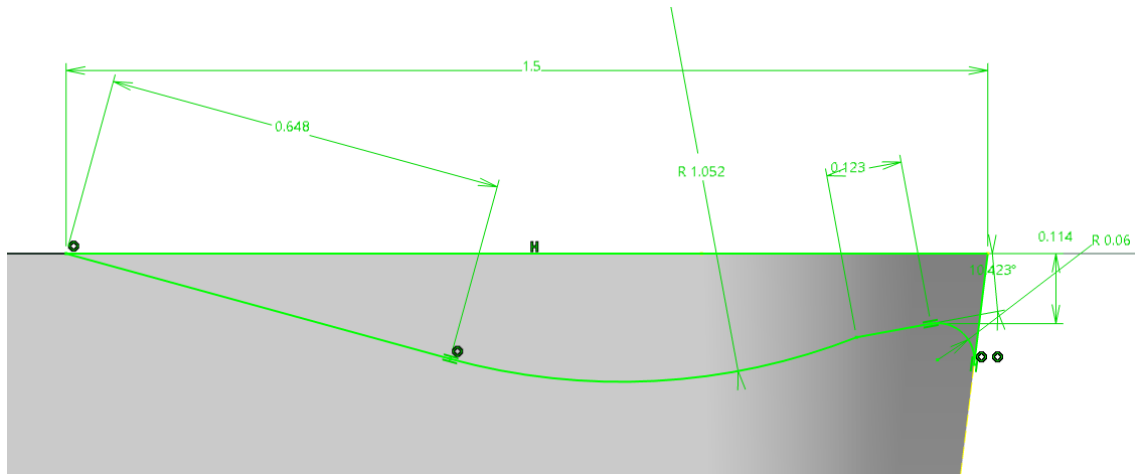
Insert CCMT09T304MM 1105 is an internal machining insert for boring operation. Figure 2.11 detected CCMT09T304MM insert rake face contour line with the basic sizes and angles. Table 2-4 list the parameters for CCMT09T304MM insert.



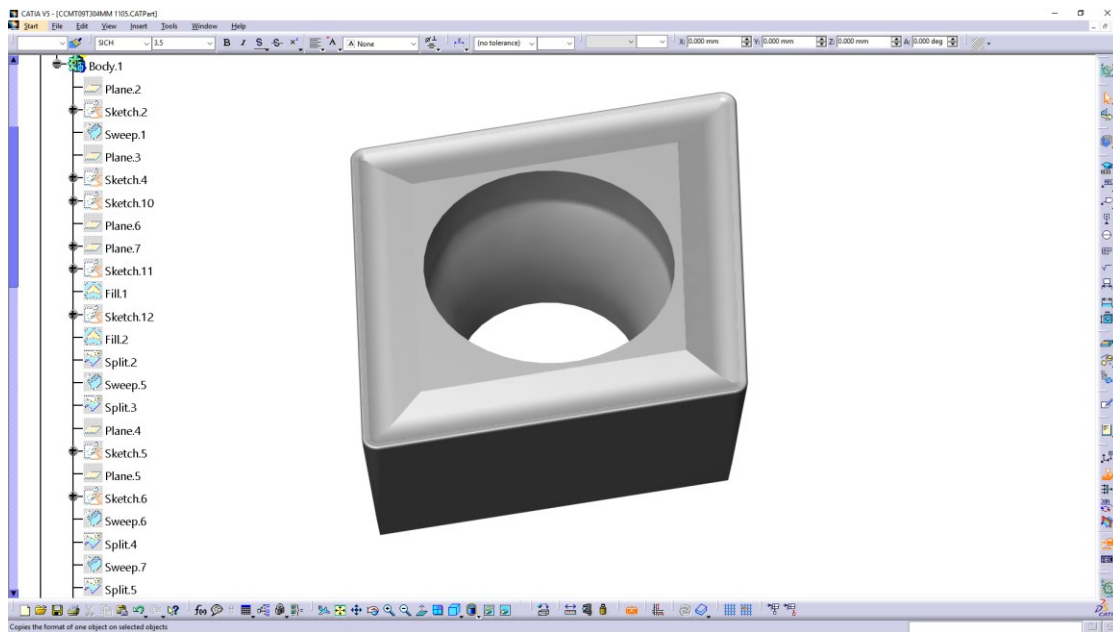
(a)



(b)



(c)



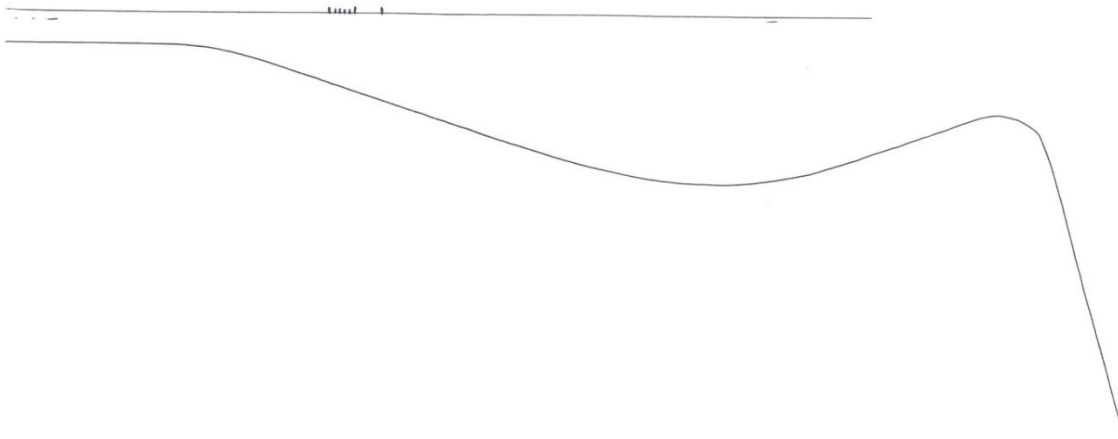
(d)

Figure 2.11 (a) An image plot of a rake face profile of the CCMT09T304MM insert, (b) Retrieving the rake face data and the cutting edge radius with the Digimazer software, (c) A sketch of the rake face and cutting edge with the CATIA software and (d) A 3-D solid model of the CCMT09T304MM insert

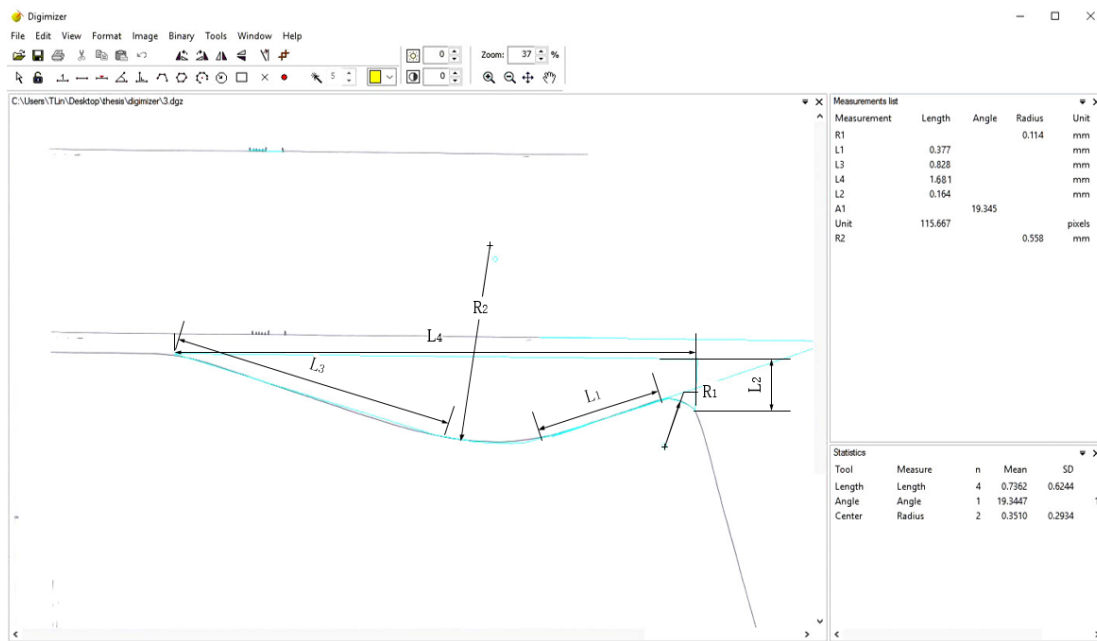
Table 2-4 The parameters of the CCMT09T304MM insert

Parameters	Definition	Value
L_1	Distance between cutting edge corner initial point with insert rake face	0.123 mm
L_2	Vertical distance between cutting edge corner initial point with insert rake face	0.114 mm
L_3	Length for back edge profile	0.648 mm
A_1	Cutting edge rake angle	10.423°
R_1	Cutting edge radius	1.052 mm
R_2	Radius of chip breaker slot	0.060 mm

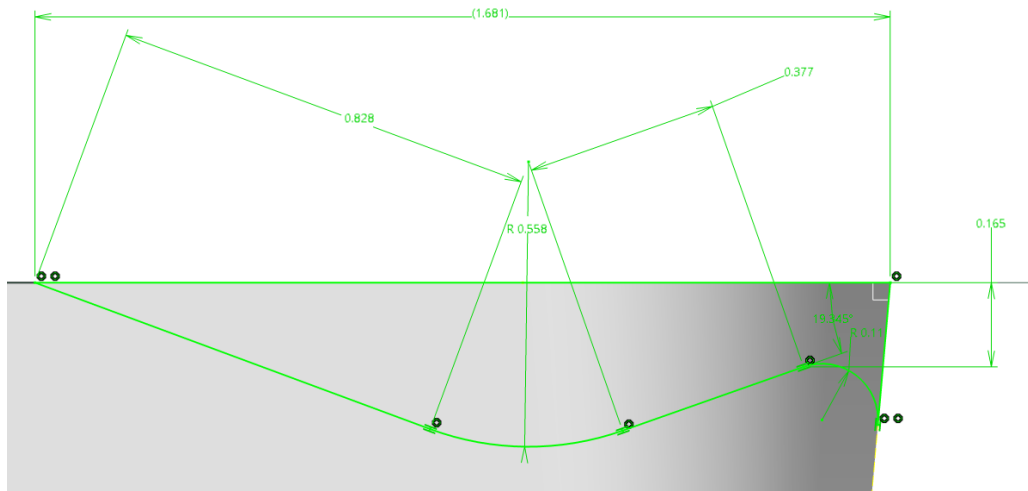
Insert VBMT160404 PC9030 is an external turning insert, the same approach is used for CAD modeling. Figure 2.12 detected VBMT160404 insert rake face contour line with the basic sizes and angles. Table 2-5 list the parameters for VBMT160404 insert.



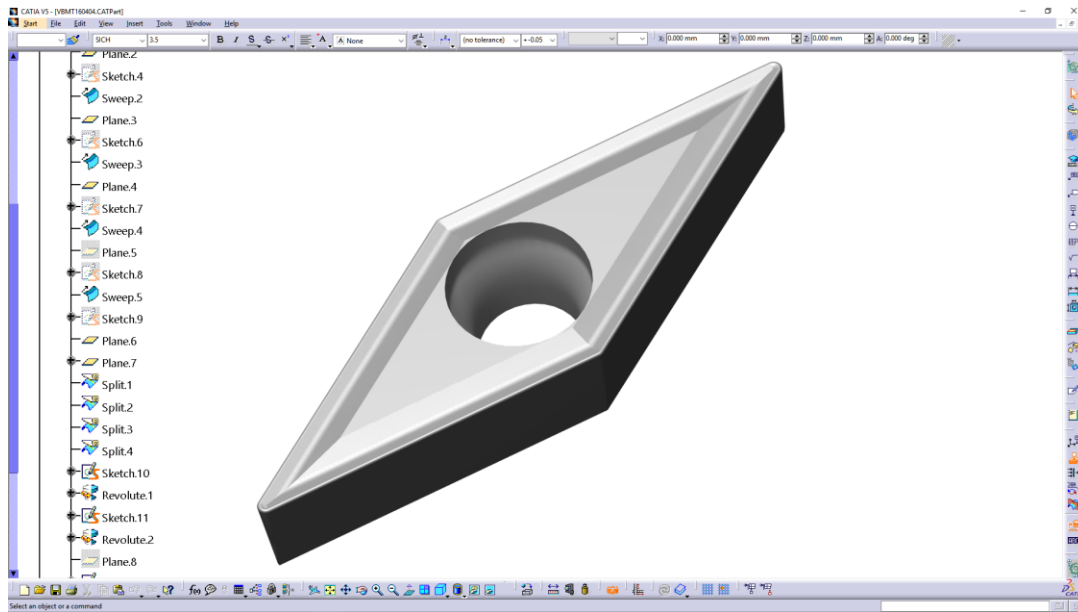
(a)



(b)



(c)



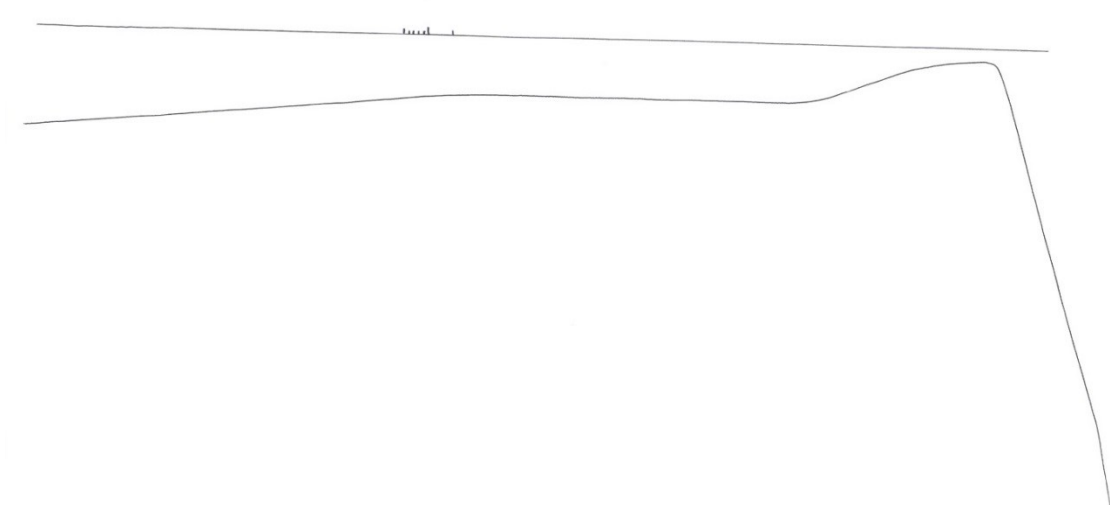
(d)

Figure 2.12 (a) An image plot of a rake face profile of the VBMT160404 insert, (b) Retrieving the rake face data and the cutting edge radius with the Digimizer software, (c) A sketch of the rake face and cutting edge with the CATIA software and (d) A 3-D solid model of the VBMT160404 insert

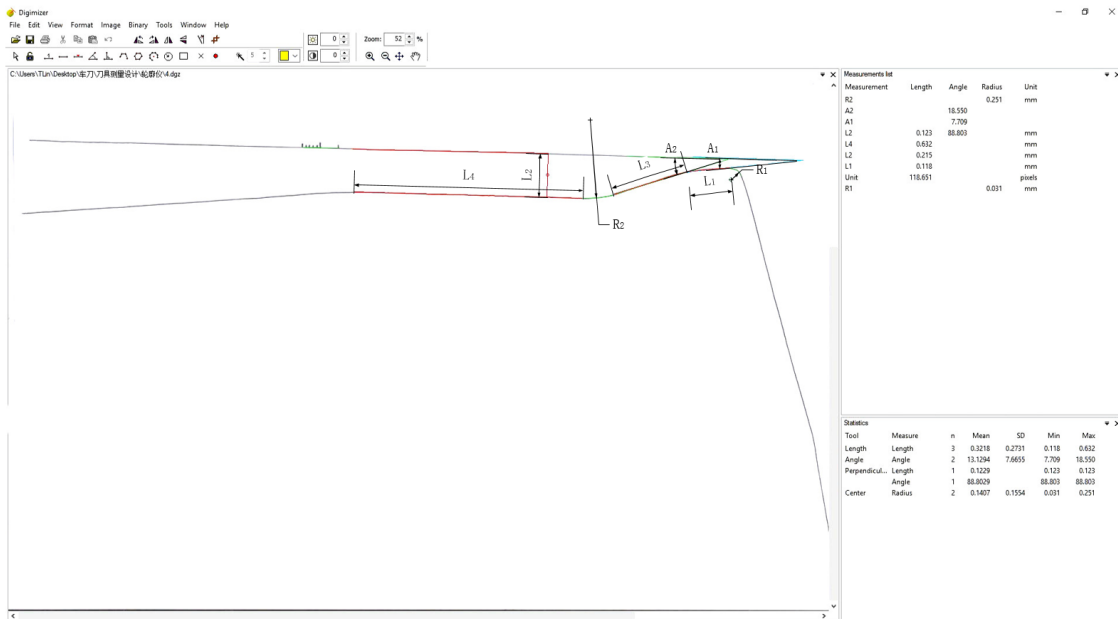
Table 2-5 The parameters of the VBMT160404 insert

Parameters	Definition	Value
L_1	Distance between cutting edge corner initial point with insert rake face	0.377 mm
L_2	Vertical distance between cutting edge corner initial point with insert rake face	0.114 mm
L_3	Length for back edge profile	0.828 mm
L_4	Cutting edge rake face length	1.681 mm
A_1	Cutting edge rake angle	19.345°
R_1	Cutting edge radius	0.114 mm
R_2	Radius of chip breaker slot	0.558 mm

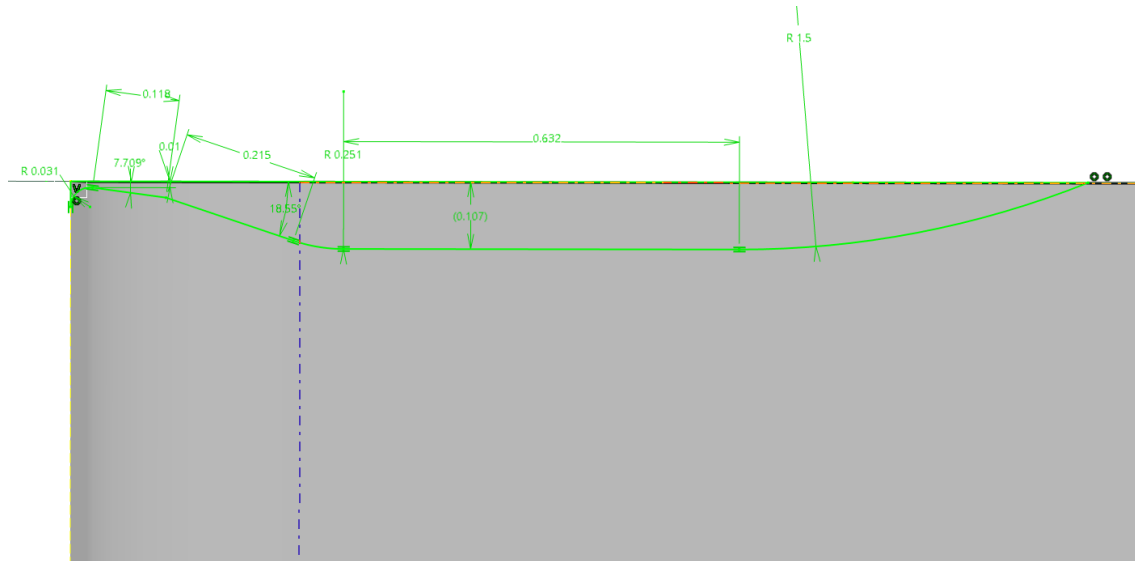
Insert DNMG150608E-4E is an external turning insert, the same approach is used for CAD modeling. Figure 2.13 detected DNMG150608E-4E insert rake face contour line with the basic sizes and angles. Table 2-6 list the parameters for DNMG150608E-4E insert.



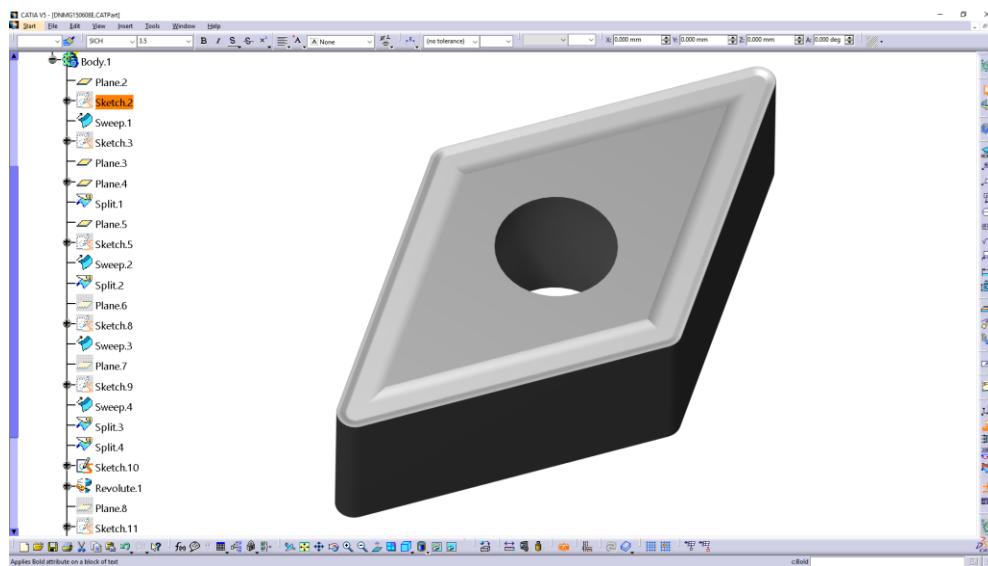
(a)



(b)



(c)



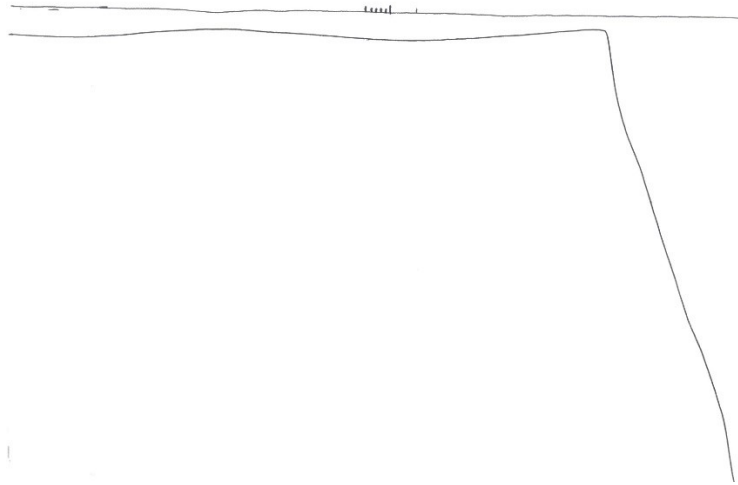
(d)

Figure 2.13 (a) An image plot of a rake face profile of the DNMG150608E-4E insert, (b) Retrieving the rake face data and the cutting edge radius with the Digimizer software, (c) A sketch of the rake face and cutting edge with the CATIA software and (d) A 3-D solid model of the DNMG150608E-4E insert

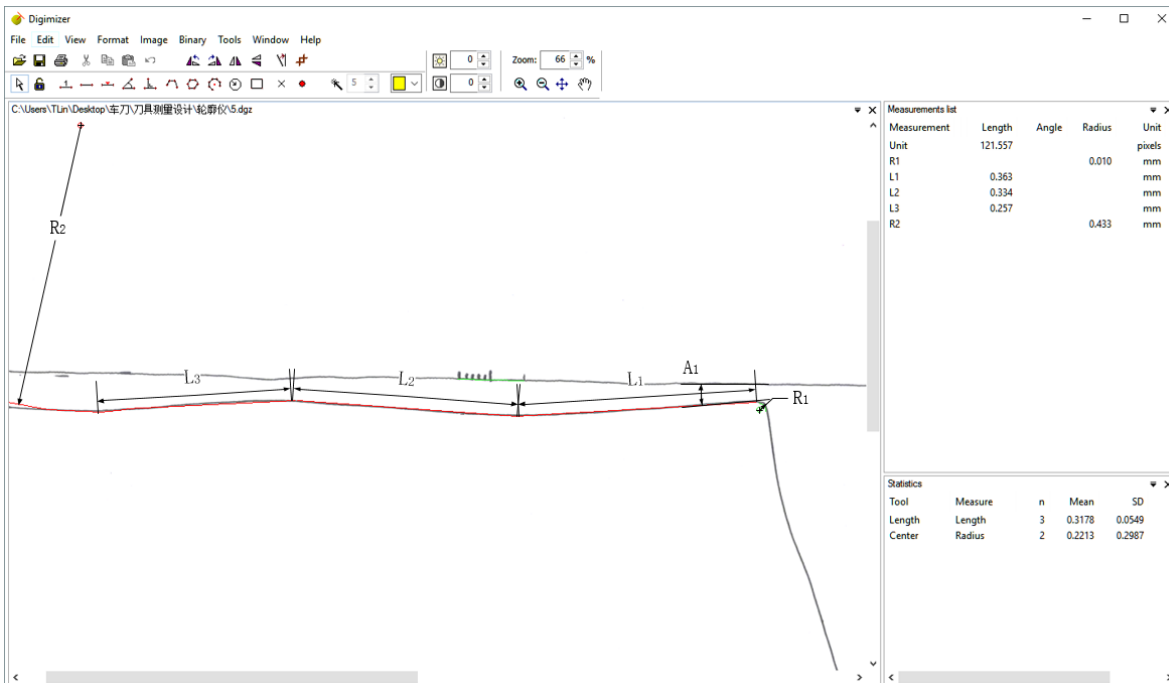
Table 2-6 The parameters of the DNMG150608E-4E insert

Parameters	Definition	Value
L_1	Length of first cutting edge rake face	0.118 mm
L_2	Vertical distance between cutting edge corner initial point with insert rake face	0.215 mm
L_3	Length of second cutting edge rake face	0.632 mm
L_4	Length for back edge profile	0.632 mm
A_1	Cutting edge first rake angle	7.709°
A_2	Cutting edge second rake angle	18.550°
R_1	Cutting edge radius	0.031 mm
R_2	Radius of chip breaker slot	0.251 mm

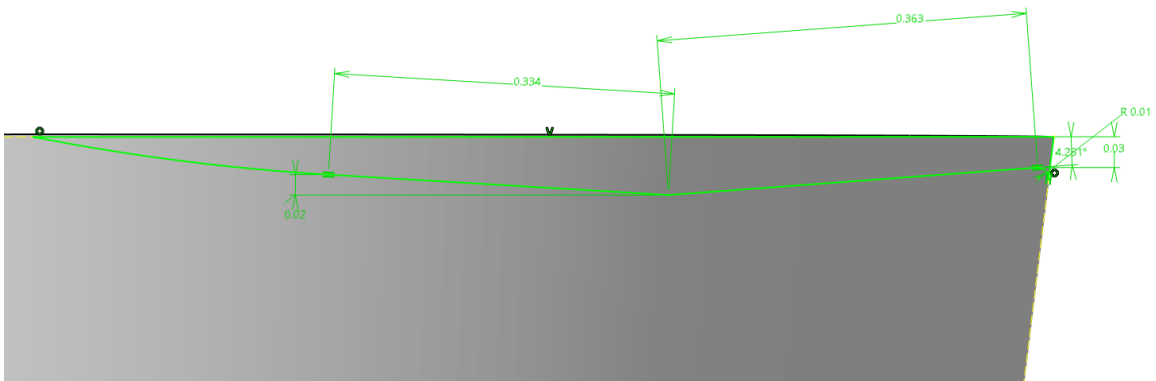
Insert N123E2 0200 R0 1105 is a grooving insert, the same approach is used for CAD modeling. Figure 2.14 detected N123E2 0200 R0 1105 insert rake face contour line with the basic sizes and angles. Table 2-7 list the parameters for N123E2 0200 R0 1105 insert.



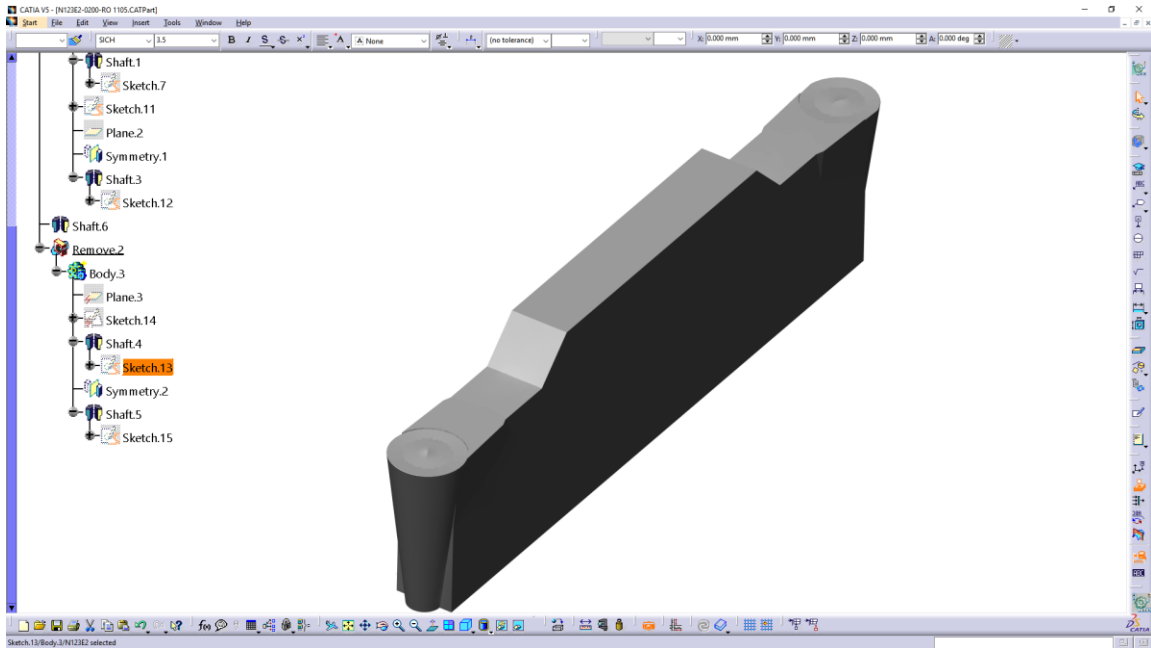
(a)



(b)



(c)



(d)

Figure 2.14 (a) An image plot of a rake face profile of the N123E2 0200 R0 1105 insert, (b) Retrieving the rake face data and the cutting edge radius with the Digimazer software, (c) A sketch of the rake face and cutting edge with the CATIA software and (d) A 3-D solid model of the N123E2 0200 R0 1105 insert

Table 2-7 The parameters of the N123E2 0200 R0 1105 insert

Parameters	Definition	Value
L_1	Length of first cutting edge rake face	0.363 mm
L_2	Length of second cutting edge rake face	0.334 mm
L_3	Length of chip breaker	0.257 mm
A_1	Cutting edge first rake angle	4.281°
R_1	Cutting edge radius	0.010 mm
R_2	Radius of chip breaker slot	0.433 mm

2.3 Measurement and Modeling of the Indexable Insert Tool Holders

An indexable insert tool holder is used to fix an insert and to set up on a lathe. The tool holder is chosen according to different machining methods such as external turning, facing and the direction of traverse. According to the ISO standard [30-31], many clamping structures of indexable insert tool holders are provided, such as clamping the insert on top, in the hole, and clamping the insert with a screw through the hole.

2.3.1 Geometry of Indexable Insert Tool Holders

There are many complex and diverse turning methods. Each of them has a suitable tool holder and insert to apply for workpiece machining. Nowadays in the industry, almost all the tool holders being used are following ISO-5610 standard [30]. And it provides some basic dimensions for standard indexable insert tool holder. Figure 2.15 indicates tool holders for different uses.



Figure 2.15 A picture of different indexable insert holders

Figure 2.16 is the ISO standard SVJBL indexable tool holder dimensions, which can be used as a holder for VBMT160408 insert. In this figure, α_n is the normal clearance angle. It's for the insert holder support slot and should be the same as the insert clearance. The h_1 is the tool holder height, which could be measured from the bottom to the top face. Letter b at the top side of the figure is the tool holder width. The l_1 is the tool holder length, which should be considered from the insert cutting edge corner to the end face of the tool holder. The l_2 is the length for tool holders head. According to the ISO-5610[30], the maximum l_2 value is given. Letter f is the distance between the insert cutting edge corner and the side face of the tool holder. The angle $0^\circ \pm 1^\circ$ in the side view A-A and B-B is the permitted range of the inclination angle and rake angle of the tool holder. Finally, s is the thickness of the insert slot without insert shim. Table 2-8 lists the parameters of the indexable insert tool holder SVJBL 2525M16.

Table 2-8 Parameters of the example indexable insert tool holder SVJBL 2525M16

Parameters	Definition	Value
α_n	Normal clearance angle	5°
h_1	Tool holder height	25 mm
l_1	Tool holder length	149.175 mm
l_2	Length for tool holders head	30.425 mm
b	Tool holder width	25 mm
f	Distance between insert cutting edge corner to the side face of tool holder	32 mm
s	Thickness of insert slot	4.76 mm

2.3.2 Measurement of Insert Slot of Indexable Insert Tool Holder by Trilinear Coordinates

Measuring Instrument

For the indexable insert tool holder, it is the tool holder insert slot that mainly affects the rake angle, relief angle, inclination angle and other angles of the turning tool when it is combined with inserts. Due to the assembly error caused by the screw clamping, the wear and deformation of the insert shim, the machining deformation, the machining error of the tool holder itself and other factors, there is some angular deviation in the tool slot of the tool holder.

In order to obtain a reliable indexable tool model for simulation, the trilinear coordinates measuring instrument is used for the measurement of the insert slot of indexable insert tool holder on the high-precision. By obtaining four points on the slot face, the slot face could be generated in a measurement software. Compared with the horizontal datum plane, we can get the relative spatial position relations between them. Figure 2.17 shows the trilinear coordinates measuring instrument.



Figure 2.17 Trilinear coordinates measuring instrument

The measurement data of the trilinear coordinates measuring instrument could be used for the modeling of the actual slot. Accompanied by the data provided by the profiler, the accurate assembly model can be established in CATIA® system and can provide the machining geometric information for the finite element analysis software Advantedge® precision cutting FEA simulation.

2.3.3 Indexable Insert Tool Holder Modeling

According to the relevant information of ISO and product sample catalog, the basic geometric model is generated. The tool holder of the indexable insert is equipped with insert shim which is the blue part shown in Figure 2.18. The test plane for the trilinear coordinates measuring instrument is the upper plane of the insert shim. And the top plane of the indexable insert tool holder is parallel to the horizontal datum plane which is provided by the tri-coordinate instrument. The size of the insert slot is related to VBMT160408 insert.

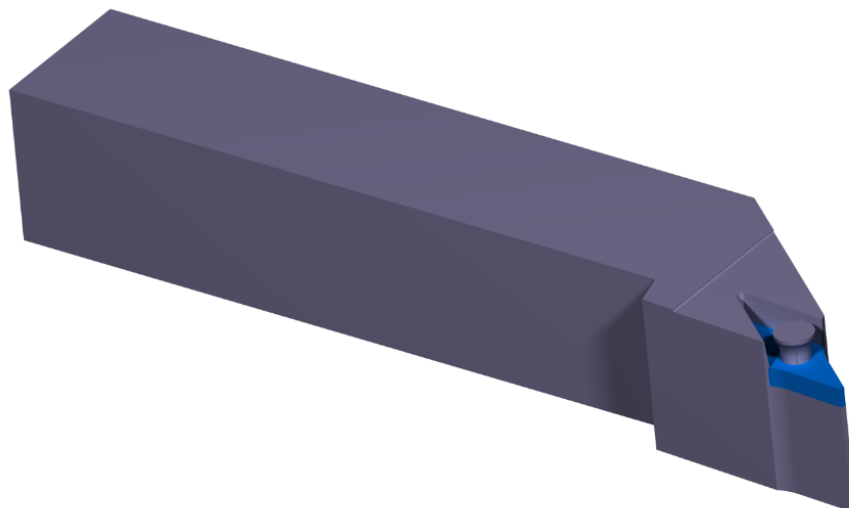
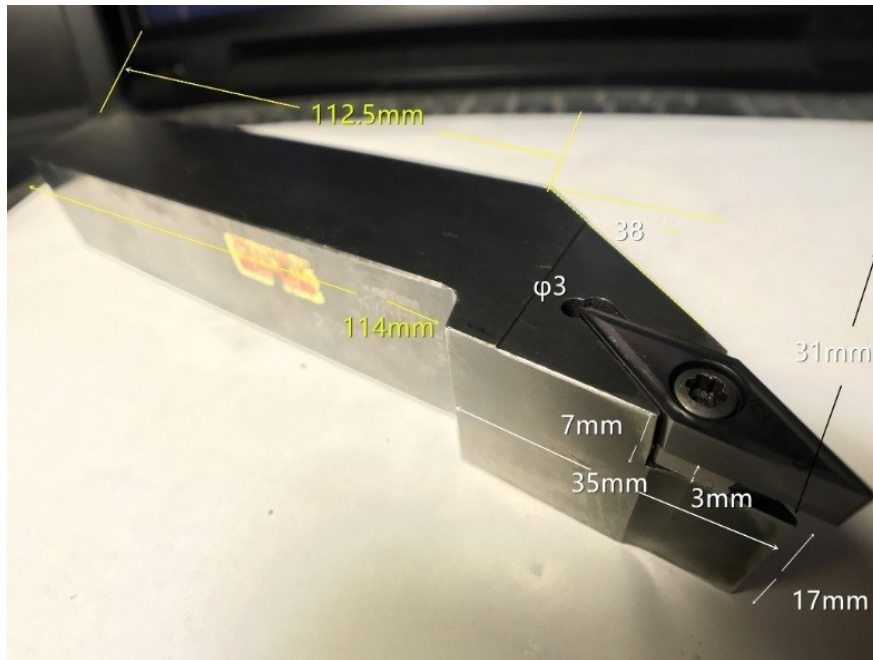
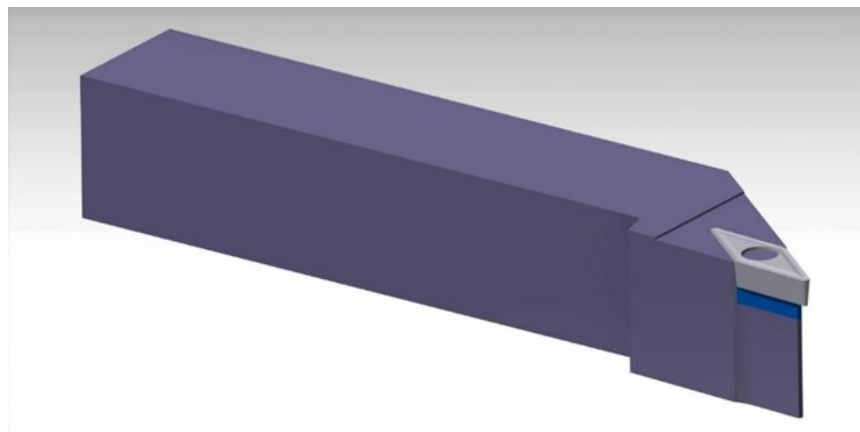


Figure 2.18 3-D model of tool holder with insert shim

All of the turning indexable inserts with indexable insert tool holders for slender shaft machining are shown below:



(a)

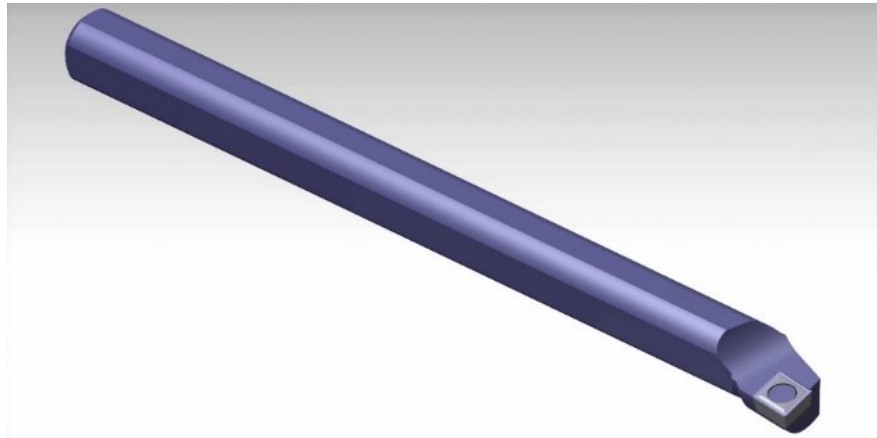


(b)

Figure 2.19 (a) A picture of a Korloy VBMT160408 insert and a Sandvik SVJBL 2525M16 tool holder, and (b) a 3-D solid model of the insert and the tool holder



(a)

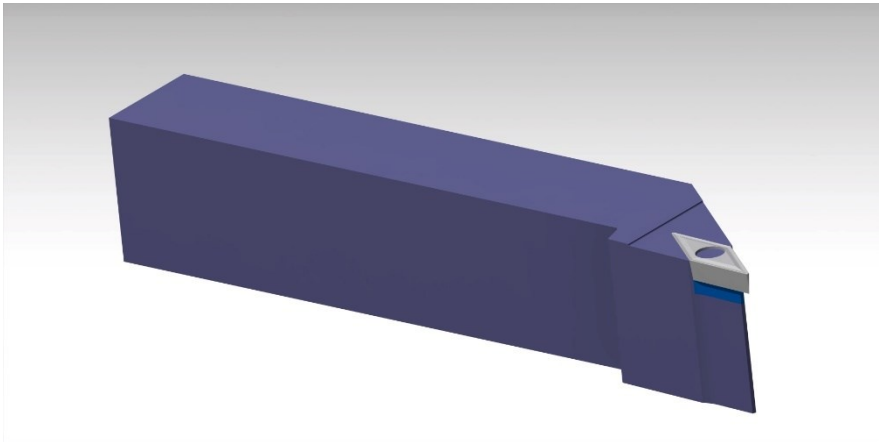


(b)

Figure 2.20 (a) A picture of a CCMT09T304 Insert and a Sandvik A16M-SCLCL09 tool holder, and (b) a 3-D solid model of the insert and the tool holder



(a)

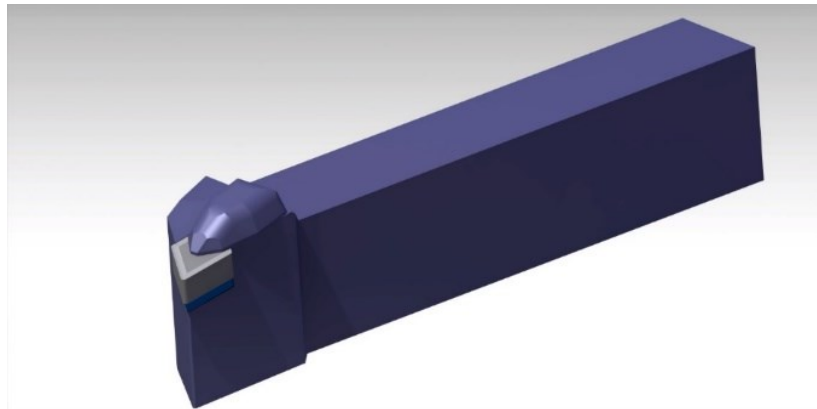


(b)

Figure 2.21 (a) A picture of a VBMT160404 Insert and a SVJBL3225 P16 tool holder, and (b) a 3-D solid model of the insert and the tool holder



(a)

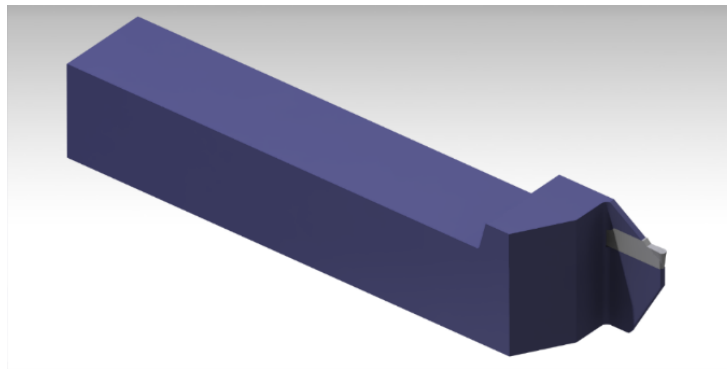


(b)

Figure 2.22 (a) A picture of a Sandvik DNMG150608 Insert and a Sandvik DDJNR3225 tool holder, and (b) a 3-D solid model of the insert and the tool holder



(a)



(b)

Figure 2.23 (a) A picture of a Sandvik N123E2 Insert and a Sandvik RF123E15-2525B tool holder, and (b) a 3-D solid model of the Insert and the tool holder

CHAPTER 3 PHYSICAL TURNING SIMULATION WITH FINITE ELEMENT ANALYSIS

3.1 Introduction of Finite Element Analysis

Finite element analysis converts continuous domains of infinite degrees of freedom into discrete domains with limited degrees of freedom. It subdivides a huge problem into a limited number of simpler and smaller problems. Finite element analysis (FEA) was initially developed from the late 1950s to early 1960s. It was mainly used for research of engineering science and technology to analyze and solve engineering mechanics, heat science, electromagnetism and other physical problems. The application of finite element analysis effectively solves a series of complex problems that cannot be solved by the conventional analytical methods. Therefore, finite element analysis software is now widely used in various scientific and engineering fields. At present, several commercial softwares, such as Thirdwave System and Abacus, are available for physical simulation of metal machining. The physical simulation can predict cutting force, cutting temperature and tool wear. Therefore, it can optimize the machining parameters, such as cutting speed, feed rate and depth of cut.

Due to the complex metal removing mechanism, many researchers made some assumptions about loads on the workpiece and the tool boundaries [6-8, 11-16]. These assumptions include (1) the cutting speed is constant, (2) the feed rate and depth of cut are constant, (3) the workpiece material is incompressible homogeneous solid, and (4) tool dynamics are not considered. In finite element analysis, the physical properties and the geometric areas of the solution domain are first determined. Then, the tool and the workpiece mesh into a finite number of elements of different sizes and shapes. The forces among the elements are passed through the nodes. Therefore, the node load matrix and the node displacement matrix of each element are super-imposed on the entire continuum. According to the node balance condition, the basic equation of stiffness is

$$[k]^e \{u\}^e = \{F\}^e,$$

where $[k]^e$ is the elemental stiffness matrix and $\{F\}^e$ is the force matrix. The $\{u\}^e$ is the solution vector for nodal displacement.

3.2 Turning Simulation with AdvantEdge Software

Currently, there are several commercial softwares available for physical simulation of metal cutting; they are Ansys, Deform 3-D and AdvantEdge. Because AdvantEdge is dedicated to metal cutting simulation, it provides customization functions for specific settings and takes into consideration tool wear, coolant and coating. Therefore, AdvantEdge is more professional in machining simulation, compared to the Ansys and the Deform software. It can analyze 2-D and 3-D workpieces and tool models to conduct the physical simulation. However, it takes more time

to analyze 3-D models. In a 2-D turning simulation, it takes about several hours to complete a simulation. In comparison, in a 3-D turning simulation, it usually takes about a week to carry out a simulation. The main flow chart of using the AdvantEdge software is plotted in the following diagram.

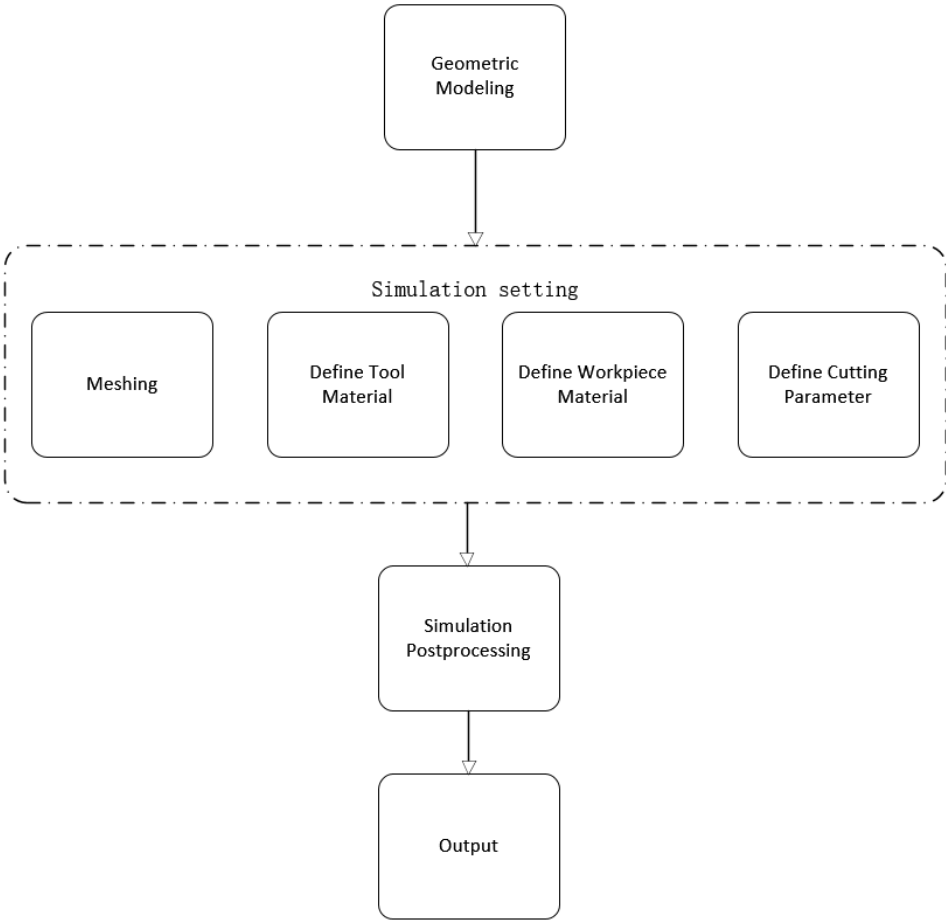


Figure 3.1 The flow chart of using the Advantedge software for machining simulation

By using AdvantEdge, the cutting force and the cutting temperature at the cutting edge and the stress and the strain of the tool rake face are predicted. With different machining parameters, the results are obtained and are compared for optimum machining parameters. The

objective is to determine the machining parameters for the maximum material removal rate and the minimum cutting force and temperature.

3.2.1 Instantaneous Workpiece Solid Model

In machining, the tool cuts a workpiece by removing the workpiece material chip by chip, and the workpiece geometry is gradually changed in this process. To conduct physical simulation at a moment, the workpiece solid model should be instantaneous to that moment. However, it is difficult to build an instantaneous workpiece solid model at every moment. In this work, a workpiece of the slender shaft is cut with five tools. The aero engine slender shaft, the three jaws chuck and the steady rest were designed in Figure 3.2. It was created in CATIA to analyze the instantaneous position and relationships of the clamping error, and for further turning simulation by MasterCAM.

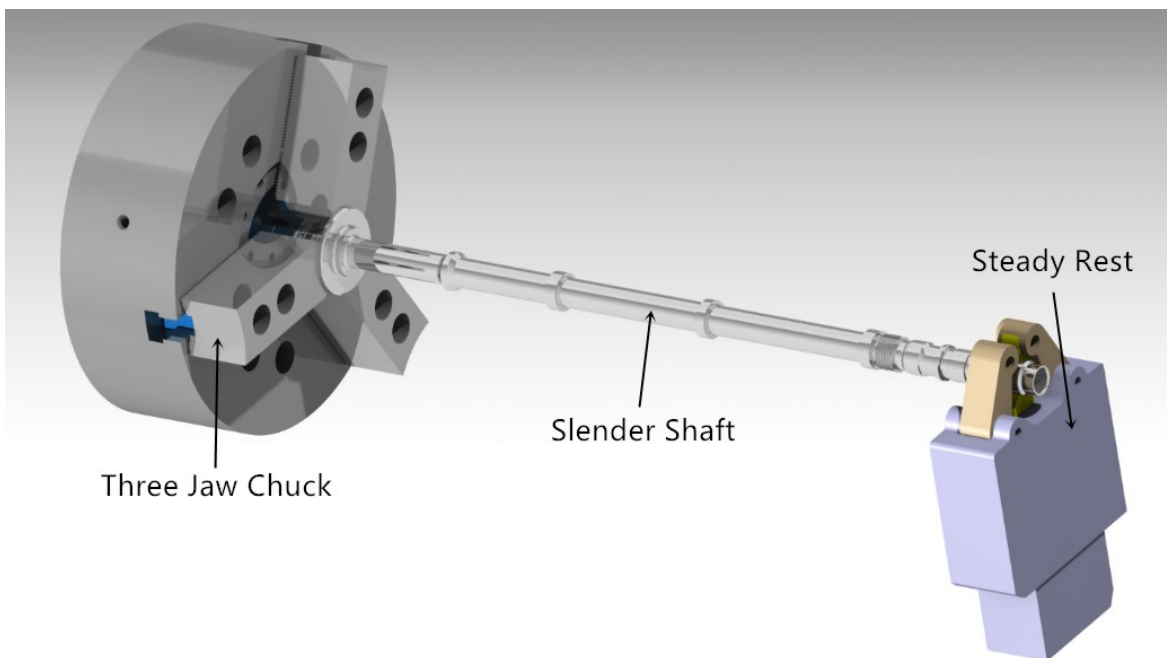


Figure 3.2 3-D models of the slender shaft turning components

Before machining, the workpiece is a bar. It is simulated in MasterCAM as shown in Figure 3.3; its outer diameter is 38 mm, and its inner diameter is 20 mm. In the first step, the workpiece is cut with No. 1 tool, and the shaft section diameter after machining is 28 mm as shown in Figure 3.4. To predict cutting force at a moment in this step, the corresponding instantaneous workpiece model should be built.

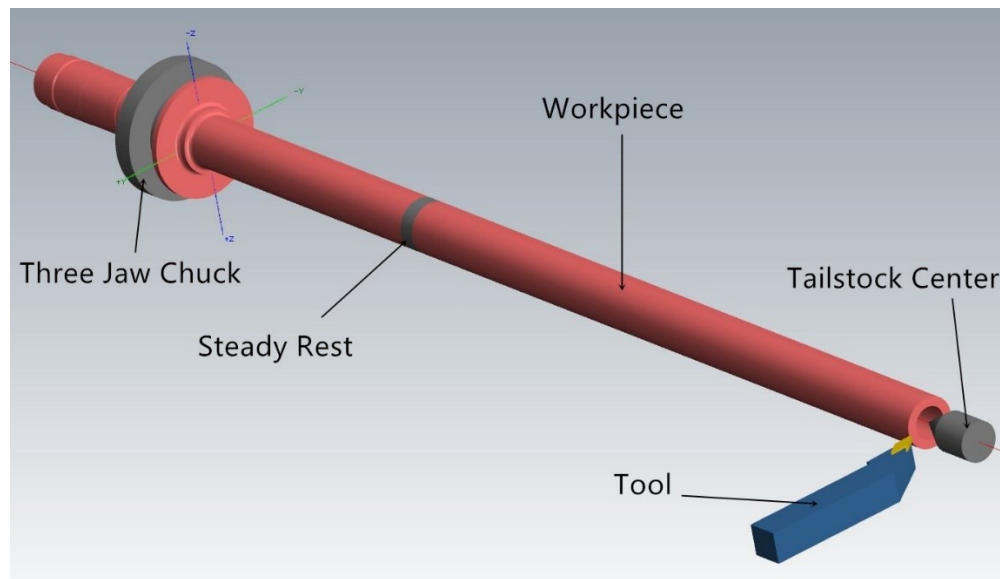


Figure 3.3 Simulation of workpiece before machining

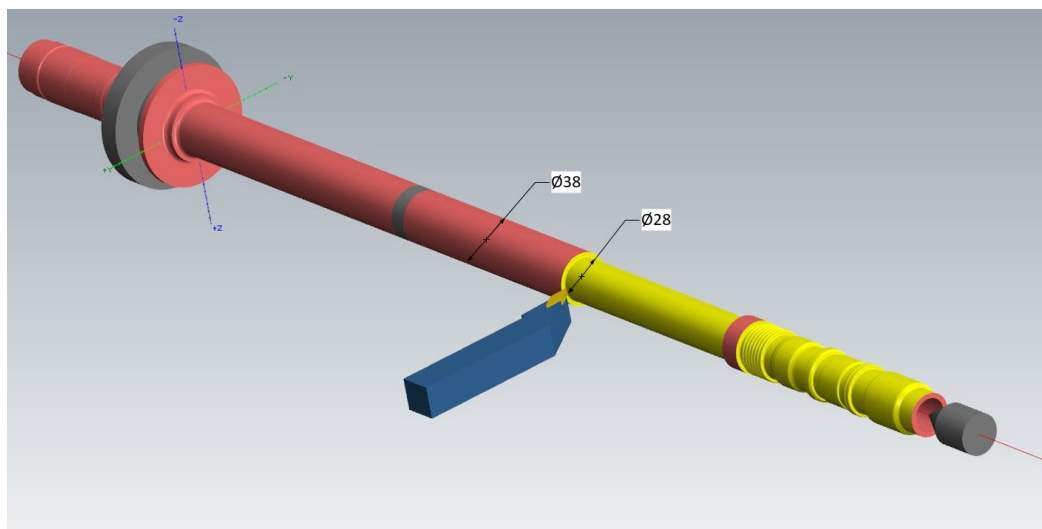


Figure 3.4 Simulation of No.1 tool turning the slender shaft

The instantaneous workpiece model is built in the following way. First, the model of the raw shaft workpiece is generated. Figure 3.5 shows a section of the model before cut. Later, in turning this section, the tool cuts the workpiece around the lathe axis. The instantaneous workpiece model is generated in two steps: (1) an envelop surface is generated by moving the insert along the helical path from the beginning to the moment of investigation, and (2) the instantaneous workpiece model is generated by subtracting the envelop surface from the raw workpiece model. The process is illustrated in Figure 3.6. The helical path is expressed as

$$\begin{bmatrix} x \\ y \\ z \end{bmatrix} = \begin{bmatrix} a \cos \theta \\ a \sin \theta \\ b\theta \end{bmatrix},$$

where a is the tool path radius, b is the feed rate, θ is the angle between tool current position and the initial position.

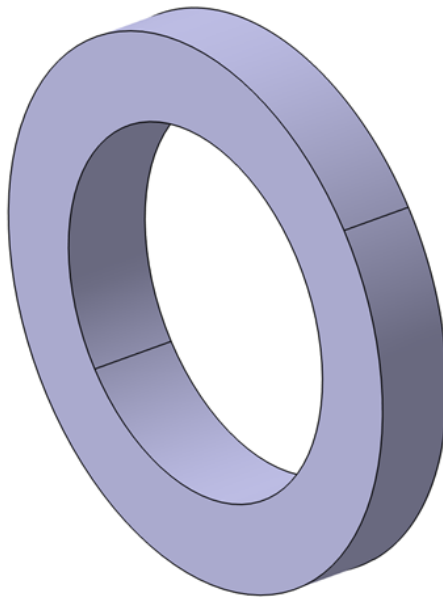


Figure 3.5 A section of the model of the raw workpiece before machining

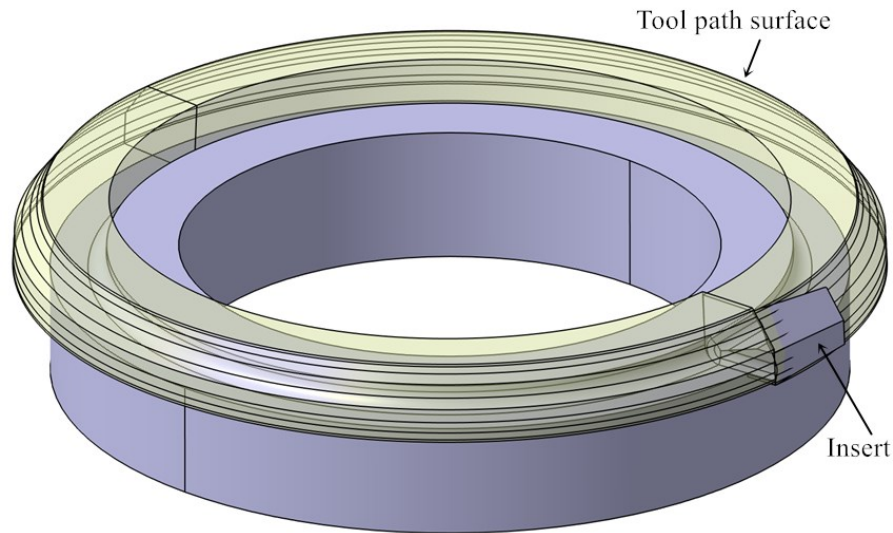


Figure 3.6 The instantaneous workpiece model is generated by subtracting the envelop surface from the raw workpiece model

In particular, the construction of an instantaneous workpiece model is explained here. The envelop surface can be generated by sweeping the insert rake face along the helical tool path. The one revolution of turning helical surface can be obtained. In this progress, the axial distance between the spiral curve starting point and the end point is feed rate per revolution f (mm/rev). By using the technique of parametric design, the STEP standard workpiece 3-D model can be automatically generated, which is convenient for a large number of FEA experiments. In this design, three main parameters are adopted. These main parameters are workpiece outer radius r , cutting depth a_p , and feed rate per revolution f (mm/rev). Parametric design is shown below in Figure 3.7.

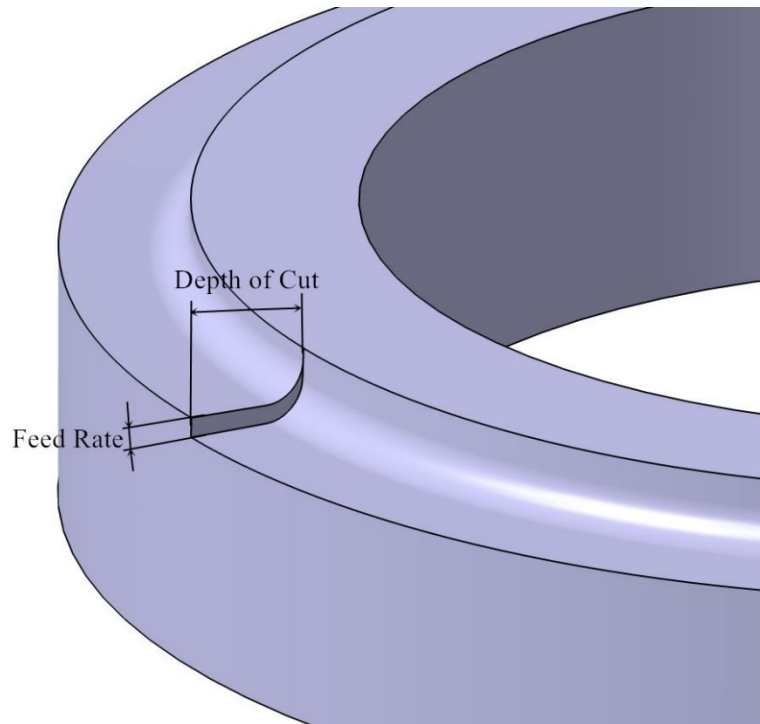


Figure 3.7 Parametric design of workpiece

After the modeling of turning workpiece is completed, it can be directly imported into AdvantEdge for finite element mesh generation. Due to the convenience of design and assembly in CAD software, it is possible to import insert and workpiece without adjusting the relative spatial position and angle relationship between blade and workpiece in AdvantEdge. This method will save much more time for repositioning. Using the secondary development program to make an automatic generation of the workpiece will greatly reduce the artificial mechanical repetition of design work.

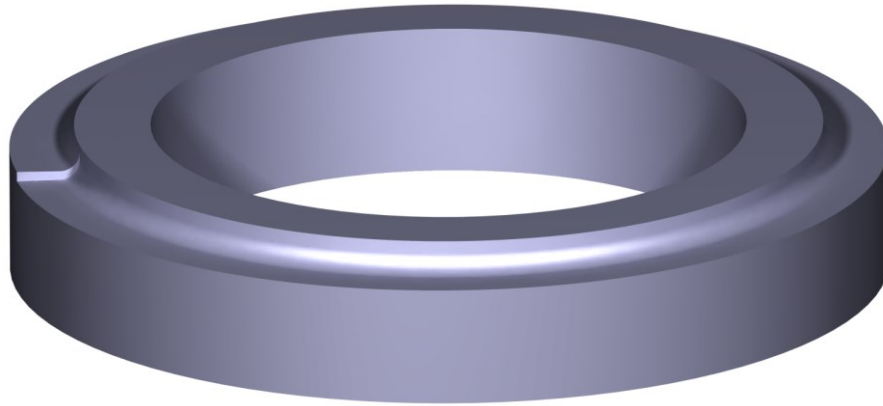


Figure 3.8 Completed simplified workpiece

3.3 Workpiece Material

For material, many researchers did a study on the constitutive model to improve the accuracy for FEA. In AdvantEdge, the user can choose the material in the preset material library or define it by many constitutive models.

3.3.1 GH4169 Performance and Machining Characteristics

GH4169 is a high-strength, corrosion-resistant super alloy which often is used in aerospace field. In American standards, it is well known as Inconel 718 series material. The highest affordable temperature for GH4169 is about 1000 ° C. Its main chemical composition and mechanical properties are as follows:

Table 3-1 Thermal conductivity and specific heat properties of high-temperature alloy GH4169

Temperature	11	100	200	300	400	500	600	700	800	1000
$\lambda(W/m \cdot k)$	13.4	14.7	15.9	17.8	18.3	19.2	21.2	22.9	23.6	30.4
$C_p(J/Kg \cdot k)$	-	450	480	481.4	493.9	514.8	539	573.4	615.3	707.4

Table 3-2 Linear expansion coefficient of high-temperature alloy GH4169

$\theta(\times 10^{\circ}C)$	2~10	2~20	2~30	2~40	2~50	2~60	2~70	2~80	2~90	2~100
$\alpha(\times 10^{-6}m/^{\circ}C)$	11.8	13.0	13.5	14.1	14.4	14.8	15.4	17.0	18.4	18.7

Table 3-3 The mechanical properties of GH4169

Property	Value (20°C)	Property	Value (20°C)
Elasticity Modulus E(GPa)	205	Tensile Strength σ_b (MPa)	1290
Shear Modulus G(GPa)	79	Yield Strength $\sigma_{0.2}$ (MPa)	1040
Poisson's ratio μ	0.30	Elongation δ (%)	15
Hardness (HB)	348	Reduction of area ψ (%)	16

GH4169 has a stable crystal structure, bringing superior mechanical properties but also increasing the difficulty of processing. Under the same cutting conditions, the cutting speed is only 10% of that of steel 45. Cutting GH4169 was investigated when the chip deformation and fracture require much more energy than steel 45. This leads to intense tool wear in high temperature and also it has high strength and high hardness. Such features make it a difficult processing material. The conventional cutting speed is 10~15m/min, and the high-speed cutting

speed is over 50m/min.

3.3.2 Constitutive Model for GH4169

The constitutive relation refers to the description of the dynamic response rule of the material's rheological stress to the parameters of strain, strain rate and temperature. For example, Hooke's law $F = kX$ is the simplest constitutive model that describes the relationship between spring deformation and tensile stress. Here F is spring force, k is its stiffness, and X is the deformation of the spring.

The constitutive equation is used to describe the properties of materials in finite element analysis, so constitutive relation modeling is the basis of rheology and finite element simulation. Since GH4169 belongs to high temperature nickel-base alloy, the Johnson-Cook (JC) constitutive model is adopted by most existing researchers' works according to its processing characteristics. The mathematical expression of JC constitutive model is:

$$\sigma = (A + B\varepsilon^n) \left[1 + C \ln \left(1 + \frac{\dot{\varepsilon}}{\varepsilon_0} \right) \right] \left[\frac{T_m - T_r}{T_m - T_r} \right]^m$$

The Johnson-Cook material model designation of material constants are as follows:

Table 3-4 Johnson-Cook material model designation of material constants

σ	Flow stress	n	Strain hardening exponent
A	Yield stress constant	m	Temperature dependence coefficient
B	Strain hardening coefficient	C	Strain rate dependence coefficient
ε	Equivalent plastic strain	T	Temperature
$\dot{\varepsilon}$	Strain rate	T_r	Room temperature
ε_0	Reference strain rate	T_m	Melting temperature
$(A + B\varepsilon^n)$	Strain hardening	$[1 + C \ln(1 + \frac{\dot{\varepsilon}}{\varepsilon_0})^m]$	Strain rate hardening
$[1 - (\frac{T - T_r}{T_m - T_r})^m]$	Thermal softening		

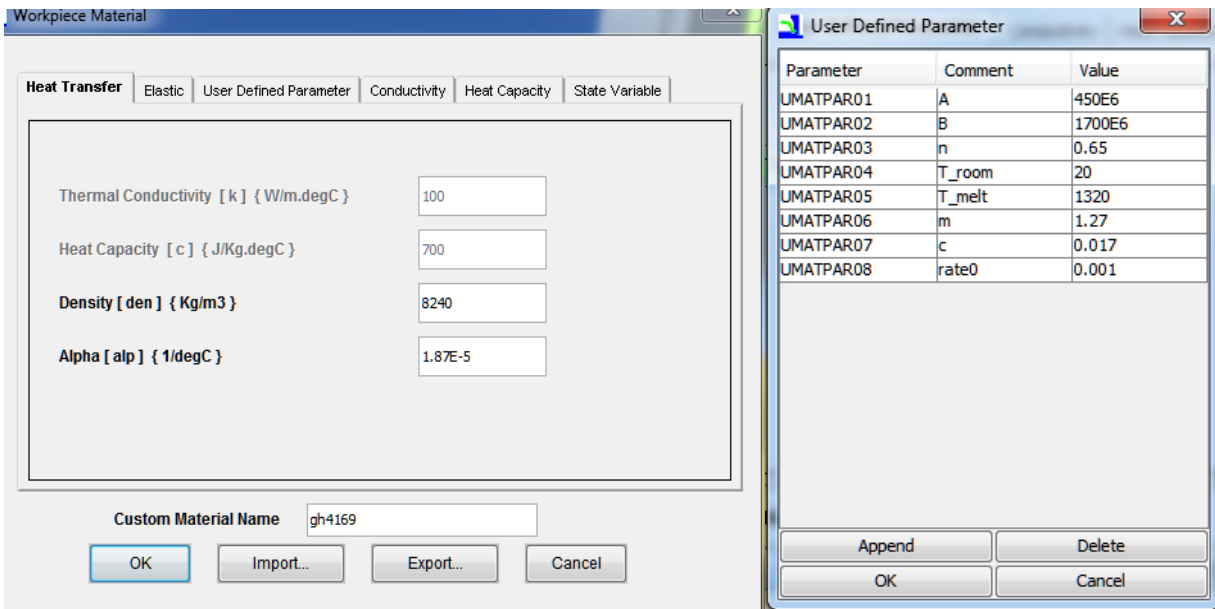
JC constitutive model is established using the split Hopkinson pressure bar(SHPB) experiment method, which is one of the most basic experimental dynamic mechanical properties of materials. In most papers [6, 11, 13, 14], the parameters of JC constitutive equation obtained through the experiment GH4169 are as follows:

Table 3-5 Parameters of JC constitutive equation for GH4169

	A	B	C	n	m	T_r	T_m
SHPB experiment	450	1700	0.017	0.65	1.3	20 C°	1320 C°
Cutting experiment	421	1224	0.0192	0.54	1.27	20 C°	1320 C°

AdvantEdge software has libraries of materials including the American standard, Japanese standard, German standard and international standard. It includes all kinds of steel, aluminum alloy, titanium alloy, high-temperature alloy and hundreds of material data. Each material file

contains the physical properties, the constitutive relation, the fracture criterion, and so on. Also, users can input relevant user-defined material models. According to the parameters obtained in the establishment of the material constitutive model shown above and the fundamental properties of the GH4169 material, the GH4169 information can be inputted into the user-defined workpiece material of AdvantEdge by modifying the file `thirdwave\advantedge\bin\usermath.dll` [32], as shown in Figure 3.9 below.



(a)

```

end forall

forall(i=1:3,j=1:3)
b_trial(i,j)=temp3x3(i,1)*df_(j,1)+temp3x3(i,2)*df_(j,2)+
temp3x3(i,3)*df_(j,3)
end forall

c
b_trace = (b_trial(1,1)+b_trial(2,2)+b_trial(3,3))
d_i_ = b_trace/3.0d0

s_trial(1:3,1:3) = b_trial(1:3,1:3)
s_trial(1,1) = s_trial(1,1) - d_i_ !b_trace/3.0
s_trial(2,2) = s_trial(2,2) - d_i_ !b_trace/3.0
s_trial(3,3) = s_trial(3,3) - d_i_ !b_trace/3.0

c
c
s_trial(1:3,1:3)= d(6)*s_trial(1:3,1:3)

yield_str = d(25) ! Initial yield stress

s_trial_norm = umat_div_norm(s_trial)

f_trial = s_trial_norm - sqrt(3.0/2.0)*yield_str

c
c Check for plastic loading
c
if ( f_trial .le. 0.0d0 ) then

sig(1:3,1:3) = s_trial(1:3,1:3)
bb(1:3,1:3) = b_trial(1:3,1:3)

else

c
c Return-mapping algorithm
c
dmu_ = d_i_*d(6)

delta_gm = f_trial/(2.0d0*dmu_)

c
c Plastic Strain
engine_s(1) = engine_s(1) + delta_gm

```

(b)

Figure 3.9 (a) User-defined JC constitutive model in AdvantEdge (b) Usermath.dll

When comparing the user-defined JC constitutive model (Figure 3.10) with the AdvantEdge material library (Figure 3.11), cutting temperature and forces are almost the same. The distribution of temperature for the user-defined JC constitutive model radiates to workpiece and chip.

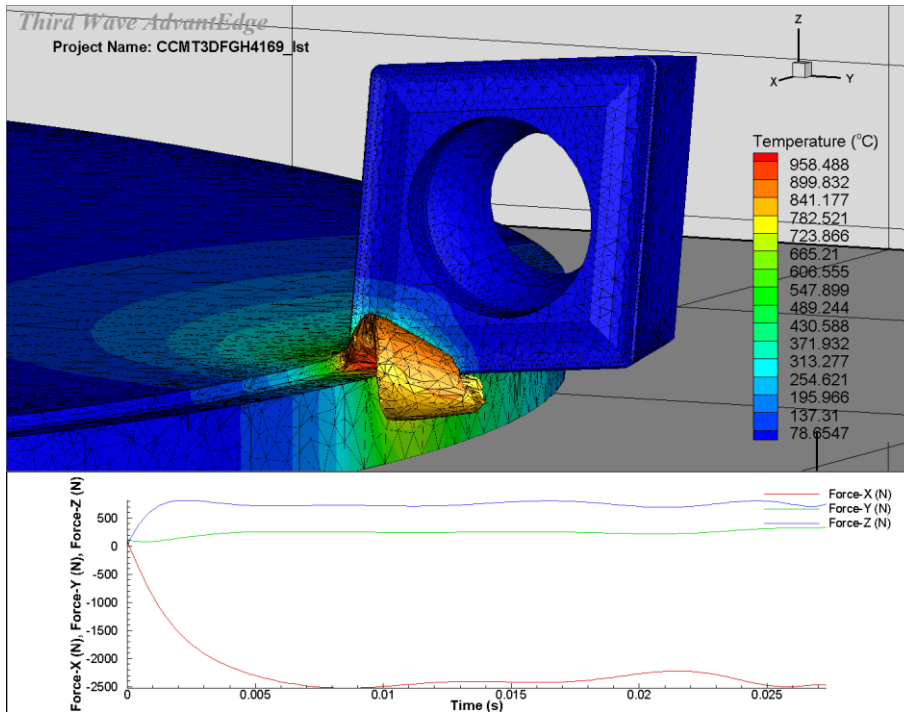


Figure 3.10 User-defined JC constitutive model simulation

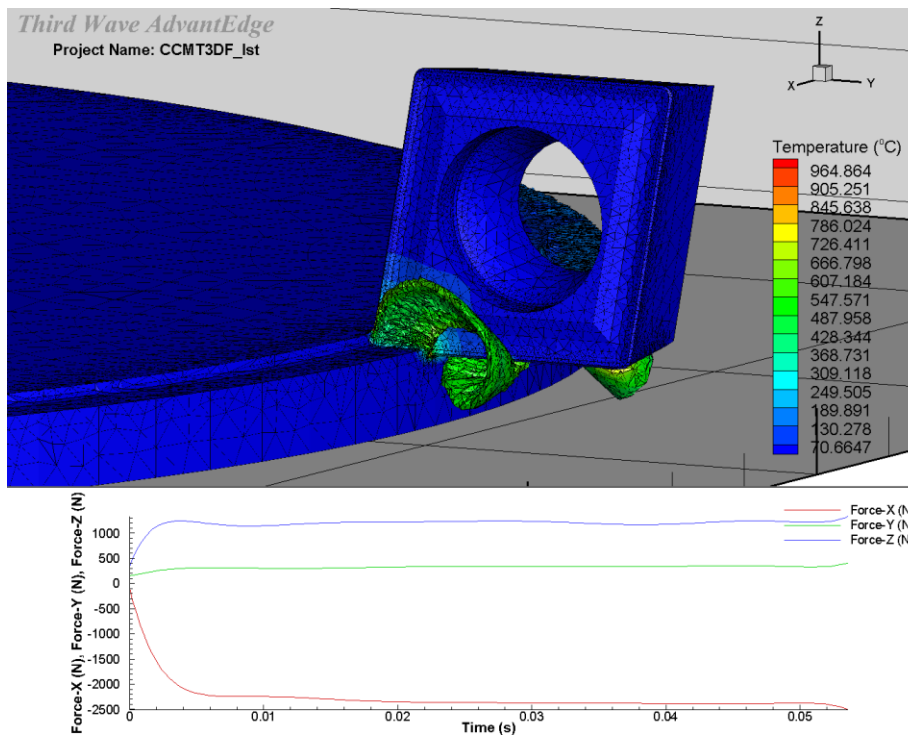


Figure 3.11 Advantedge material simulation

3.4 Tool Material

For tool material, we assume it has a perfectly elastic material model for the tool. In the library of the software, we can define the material but there are no details of a material model for the tool. Figure 3.12 shows the tool material Carbide in AdvantEdge.

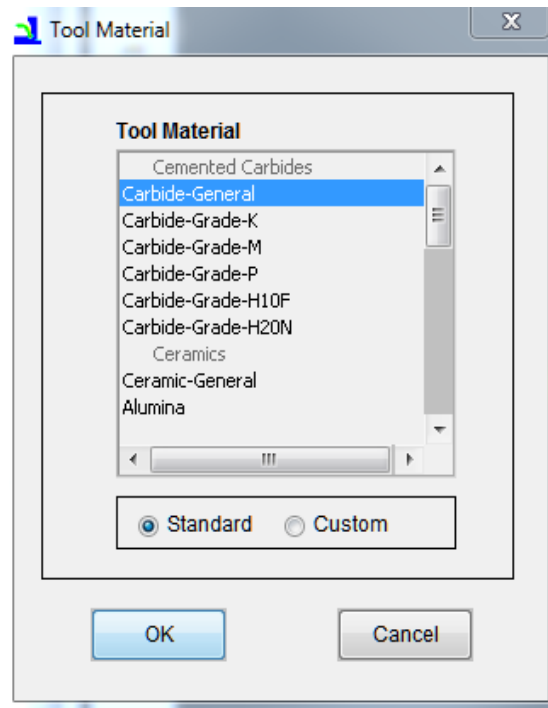


Figure 3.12 Tool material

3.4.1 Coating Material for Insert

Typical thickness of indexable turning tool coating is 6-12 μm . As Figure 3.13 shows, AdvantEdge provides TiN, titanium nitride, Al_2O_3 , alumina, TiC titanium carbide, and titanium TiAlN nitrogen aluminized coating options for simulation. The coating can also be customized for finite element analysis.

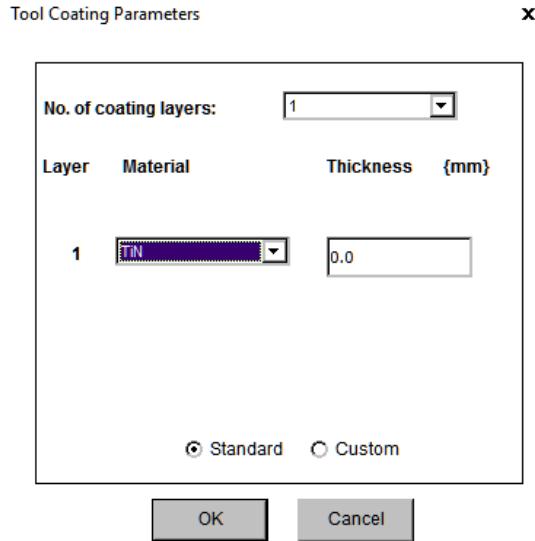


Figure 3.13 Tool coating

3.5 Meshing in AdvantEdge

Figure 3.14 shows the AdvantEdge meshing system. The meshing automaticity and re-meshing automaticity are very high. Generally, the mesh quality for the STEP model is excellent, which is very well customized for cutting simulation. It provides the precision adjustment function in the mesh refinement workbench according to the complexity of the cutting tool and of the workpiece. It can focus on the important parts in order to improve the accuracy of the finite element simulation. In this study, the function is used for improving the precision of the indexable insert main cutting edges.

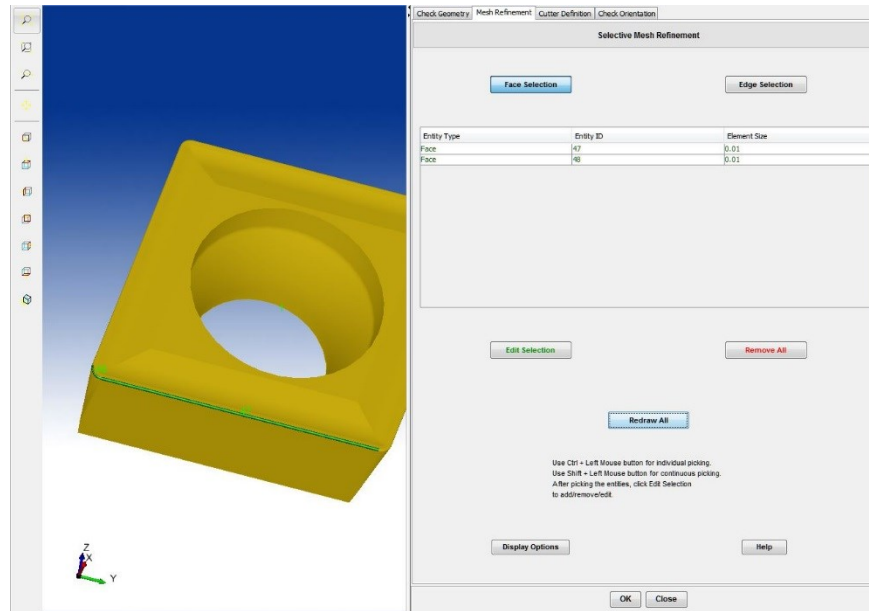


Figure 3.14 Tool meshing

The figure 3.15 shown below is a demonstration for the 3-D insert model under different softwares. In AdvantEdge, the force X is the force on cutting speed direction, the green arrow in Figure 3.15. Force Y is the force on the workpiece bar radius direction, the violet arrow in Figure 3.15. Force Z is the force on feed rate direction, the red arrow in Figure 3.15.

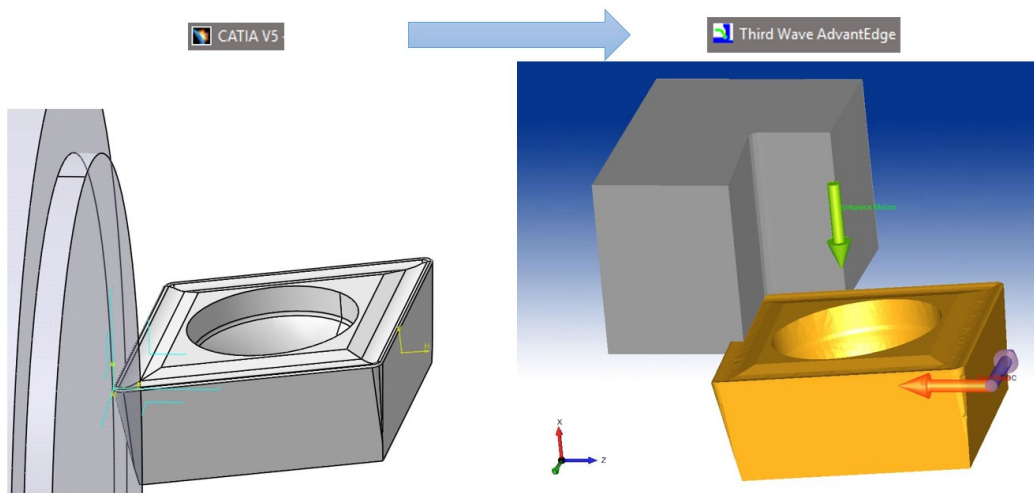


Figure 3.15 CATIA to AdvantEdge

In order to diminish simulation time, the insert model is being simplified by half of cutting edge, which is used in simulation as shown in Figure 3.16. It will not influence the result in accuracy by setting up boundary conditions on end faces.

As Figure 3.16 shows, the faces 4&7 are cutting edge surfaces, which have a small radius for improvement of intensity. In order to find the relationship between mesh areas on tool rake face and simulation results, an experiment was designed to define the suitable tool mesh areas. Table 3-6 shows the tool mesh areas experiment.

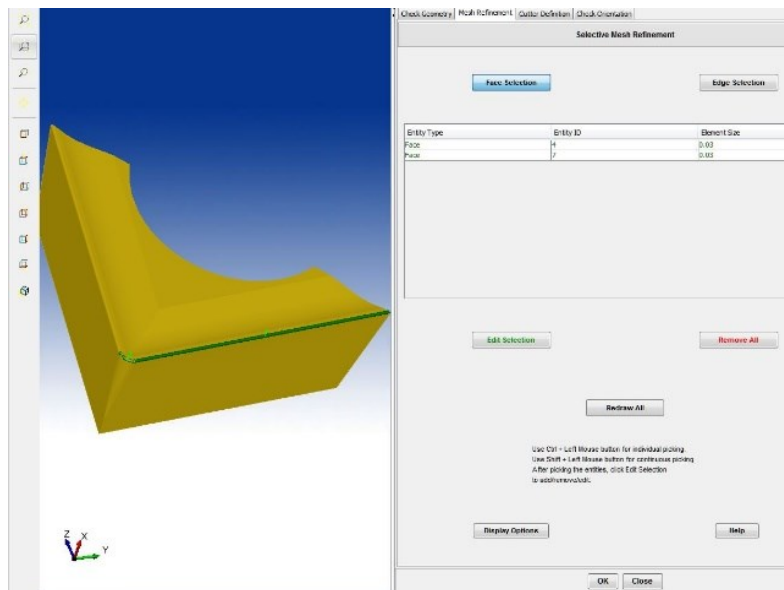


Figure 3.16 Simplified insert model

Table 3-6 Parameters of JC constitutive equation for GH4169

Experiment No.	Mesh area	Precision
1	Cutting edge corner (face 4)	0.01mm
2	Mean cutting edge (face 7)	0.01mm
3	Cutting edge and corner (face 4&7)	0.01mm

Figure 3.17 shows the result of the experiment. By decreasing the element size for specified areas, the force relying on cutting speed direction was decreased by 20%. And the faces on cutting edge influenced the result of temperature and forces dramatically. Also, the rake faces and the body faces of the insert have been tested. Compared with cutting edge faces, the body faces only increase precision of the result by a small amount, and they also add a large number of extra computation time.

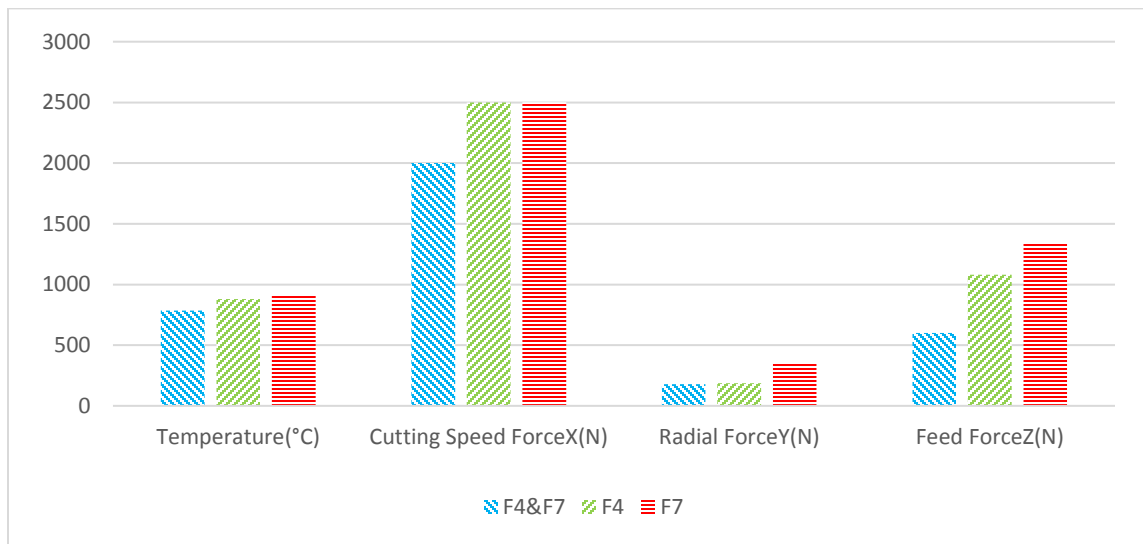


Figure 3.17 Relationship between mesh areas of insert and simulation result

After revealing the relationship between mesh areas of insert and simulation results, the next step of the research is the sensitive rate test shown in Table 3-7. It is the relationship between tool mesh precision and FEA results.

Table 3-7 Sensitive rate test for tool mesh precision

No.	Tool mesh(mm)	Temperature(C)	ForceX(N)	ForceY(N)	ForceZ(N)
1	0.09	970	2522	360	1545
2	0.08	1100	2474	352	1402
3	0.07	987	2325	330	1242
4	0.06	1009	2213	256	851
5	0.05	1093	2146	194	788
6	0.04	784	1894	166	646
7	0.03	879	1854	161	632
8	0.02	872	1548	151	560
9	0.01	889	1339	144	573

Figure 3.18 shows the results of the sensitive rate test for the precision of insert. By improving the precision for cutting edge areas from 0.09mm to 0.01mm, the force relying on cutting speed direction can be decreased by 46%. Also, force Y and Z decrease when precision increases. For temperature, it did not change too much compared with forces. Therefore, by increasing the mesh precision, the lower forces and temperature will be obtained with less error with the actual experiment.

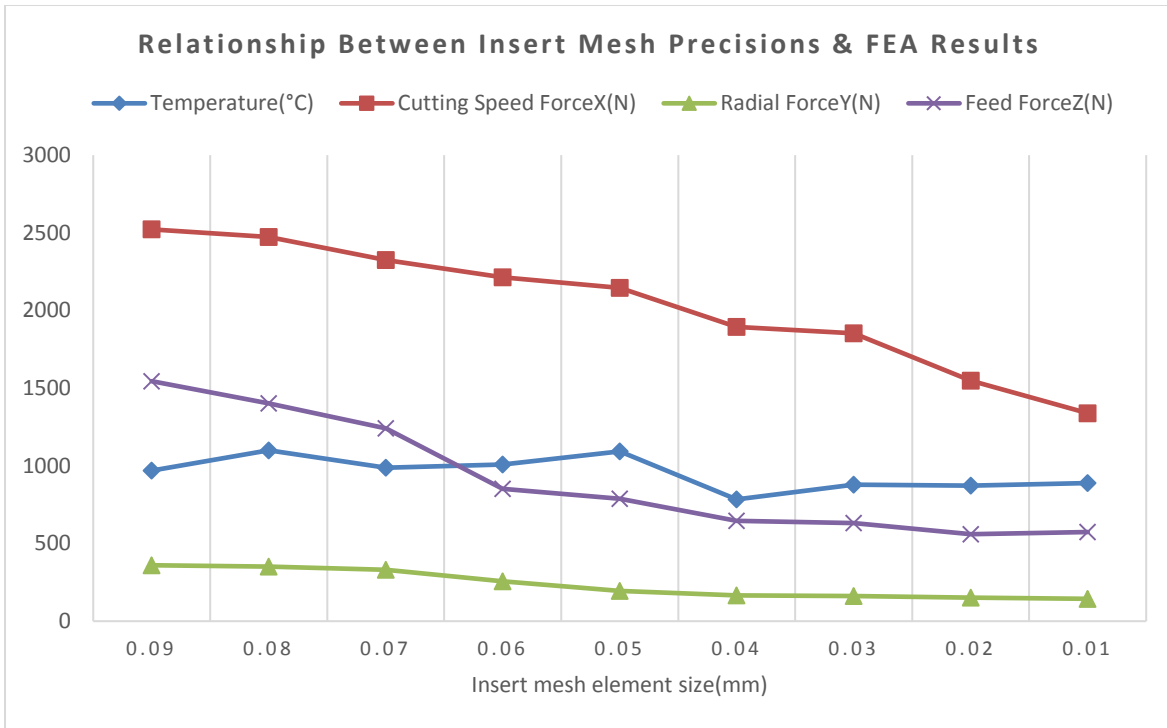


Figure 3.18 Relationship between mesh precisions of insert

For the workpiece, we can also set the precision of the mesh. Theoretically, different workpiece precisions will also influence the calculation results. When machining parameters are minimal, such as when the feed is 0.01mm, the workpiece mesh precision will not dramatically influence the results compared with cutting edge mesh precision. Figure 3.19 shows the mesh setting for workpiece.

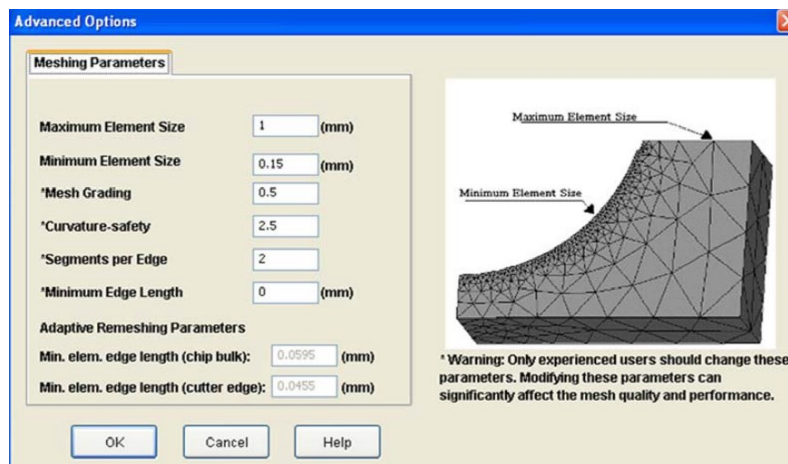


Figure 3.19 Mesh setting for workpiece

The following figure is the sensitivity test diagram of the workpiece accuracy and simulation results. As shown in the figure, with the increase of mesh precision from 0.5mm to 0.1mm, the experimental results have not changed dramatically.

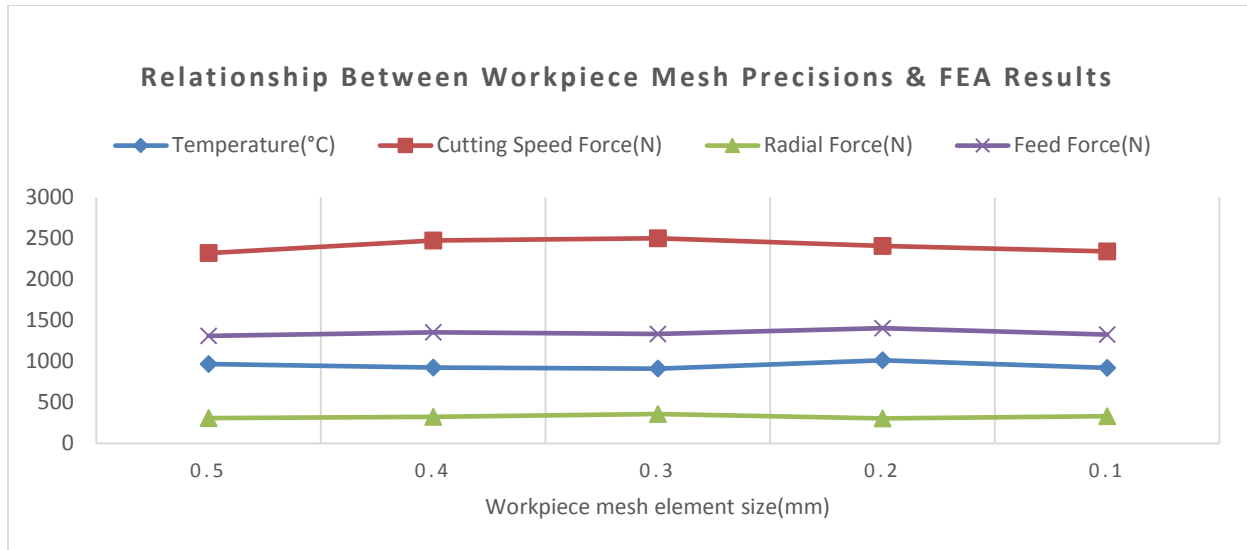
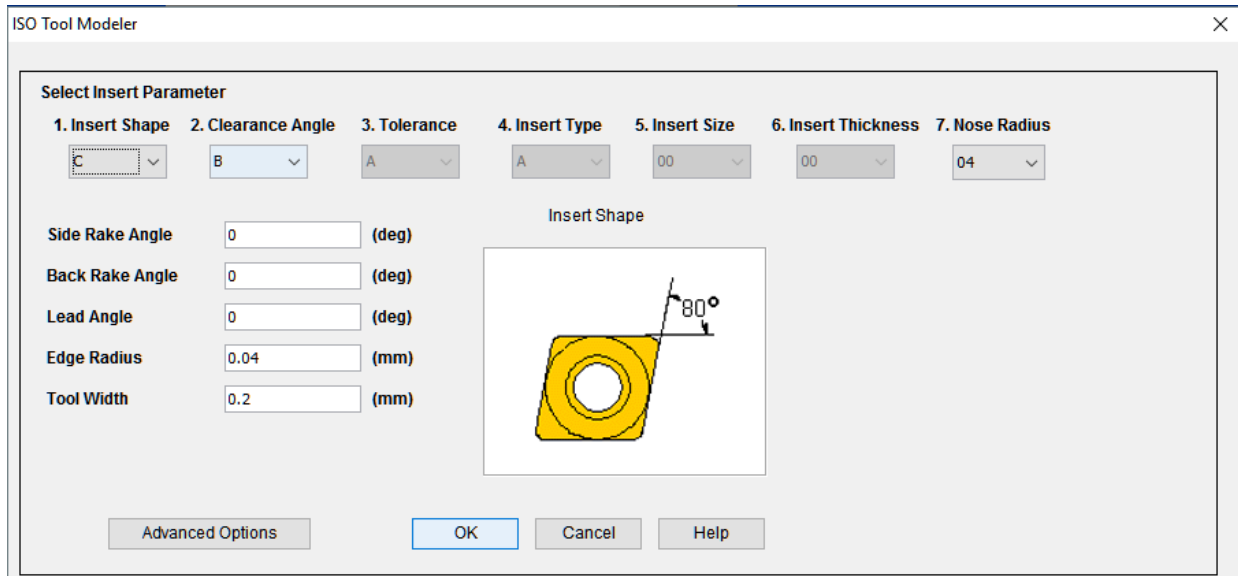


Figure 3.20 Sensitive test for workpiece mesh precision

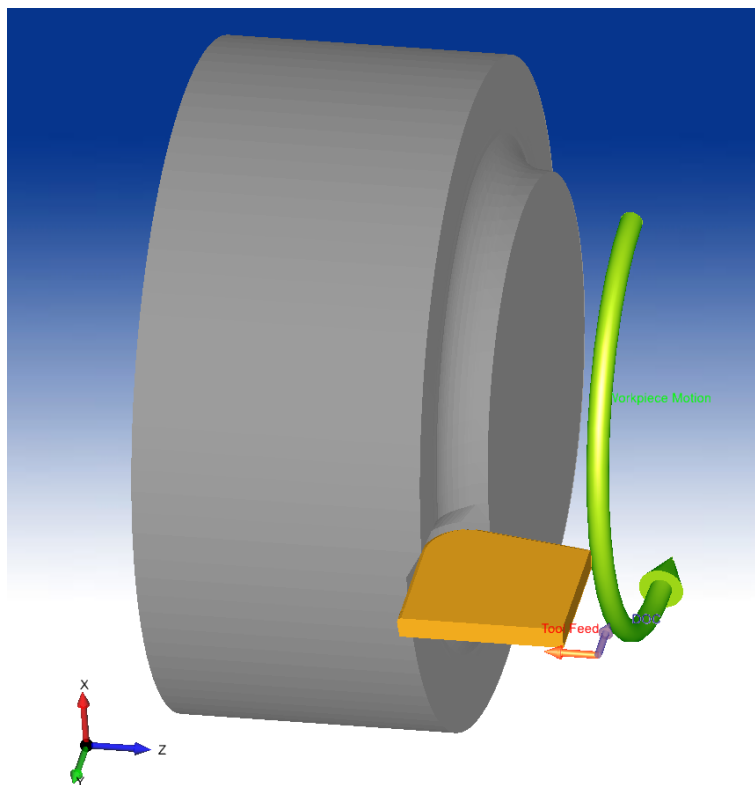
In conclusion, due to the meshes that are automatically generated by AdvantEdge, the meshing precision settings significantly affect the results. The improvement on main cutting edge mesh precision can dramatically reduce cutting force and reduce more than 60% of the error compared with the real test.

3.6 Tool Relocation

AdvantEdge has ISO Tool Modeler as shown in Figure 3.21(a). It can easily set geometry for inserts, but it can't be used for accurate simulation because of the lack of rake face geometry as shown in Figure 3.21(b), which makes the output dramatically different from many previous researches.



(a)



(b)

Figure 3.21 (a) ISO Tool modeler (b) 3-D model of AdvantEdge built-in insert and workpiece

When importing the STEP file of insert 3-D model, the AdvantEdge needs the user to manually relocate the cutting tool following the required orientation as shown in Figure 3.22.

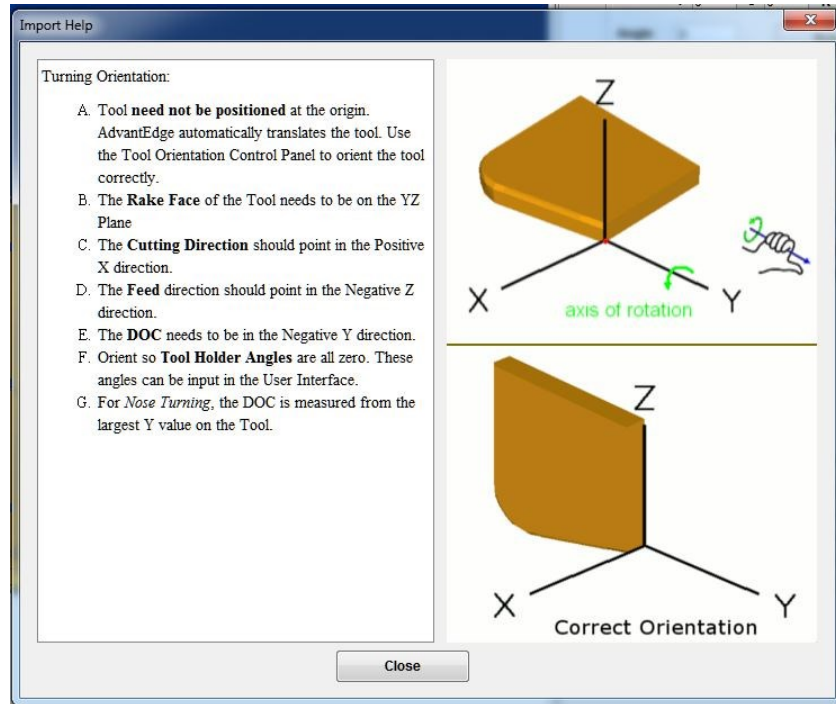


Figure 3.22 Turning orientation in AdvantEdge

The software uses a very complex way to force the user to define tool and workpiece location in their system. Also, there is no tool to measure distance and angle to verify whether the location is correct or not. Therefore, the better way is using CATIA to assemble the workpiece and the tool, and then to import them as a combined group.

3.7 Finite Element Simulation Experiment Design

In this chapter, the discussion about FEA experiment design for turning was provided.

According to the indexable insert recommendation parameters and the limitations from the lathe machine center itself, the orthogonal experimental design method has been adopted to analyze the effects of three cutting parameters on the simulation result.

3.7.1 Selection of Cutting Parameters

At present, the high temperature nickel base alloy GH4169 was investigated by workers through cutting experiment or processing experience to obtain the appropriate cutting parameters. Generally speaking, through the experience or test method, the cutting parameters still have optimization room. According to the official recommended parameters, ISO standards and factory processing parameters, a suitable cutting speed V_c , for example insert VBMT160408, is between 50-80m/min. When selecting the cutting depth of turning, we set the cutting depth of the simulation experiment between 0.9mm and 2.5mm based on the official recommended parameters and the blade tip radius. In order to choose a suitable feed rate, we should consider the high requirements for aviation slender shaft surface roughness and surface integrity. Also, the feed rate should improve precision as far as possible instead of focusing on machining efficiency. Therefore, the feed rate range is between 0.1 ~ 0.25 mm per revolution.

3.7.2 Orthogonal Experimental Design

The Taguchi Method, also called Orthogonal Experimental Design method, is a statistical method developed by Genichi Taguchi [28] to be used to improve the quality of manufactured goods. The Orthogonal Experimental Design (OED) method is usually used to find the best combination of factor levels that can be found in several tests to study the effects of several

factors simultaneously. The cutting speed v , the feed rate f and the cutting depth a_p will influence the quality of manufactured workpieces. Finding optimized parameters for a specific machining toolpath is time-consuming for the simulation. Therefore, the OED method is the ideal way to decrease simulation time. The cutting experiments are using the Korloy® VBMT160408 carbide insert with a grade of PC9030 for the machining of GH4169 high temperature alloy bars. The Table 3-8 shows cutting parameters and their levels for the OED method. All cutting parameters are independent.

Table 3-8 Cutting parameters and their levels

Cutting Parameter	Unit	Level 1	Level 2	Level 3
Cutting speed	<i>m/min</i>	56.5	67.8	79.2
Feed rate	<i>mm/rev</i>	0.1	0.17	0.25
Cutting depth	<i>mm</i>	0.9	1.7	2.5

After selecting suitable parameters with their levels, the degrees of freedom (DOF) should be computed for selection of orthogonal arrays. It's defined as the number of observations in the data that are free to vary when estimating statistical parameters. For example, for cutting speed, there are three levels and two degrees of freedom. The next step is to select a suitable orthogonal array to obtain requirements. In this study, an orthogonal array of four columns and nine rows L_9 was used. It can study the entire parameter range using only nine experiments. Because there are four columns for the L_9 orthogonal array, three of the columns are cutting parameters, and the other column of the array is empty for error of experiment. And the orthogonal array will remain

the orthogonality. In the orthogonal array, numbers 1,2 and 3 for parameters A,B,C and D are used to indicate the levels of parameters. The L_9 orthogonal array is shown in Table 3-9.

Table 3-9 L_9 orthogonal array

Experiment No.	A Cutting speed	B Feed rate	C Depth of cut	D Error
1	1	1	1	
2	1	2	2	
3	1	3	3	
4	2	1	3	
5	2	2	1	
6	2	3	2	
7	3	1	2	
8	3	2	3	
9	3	3	1	

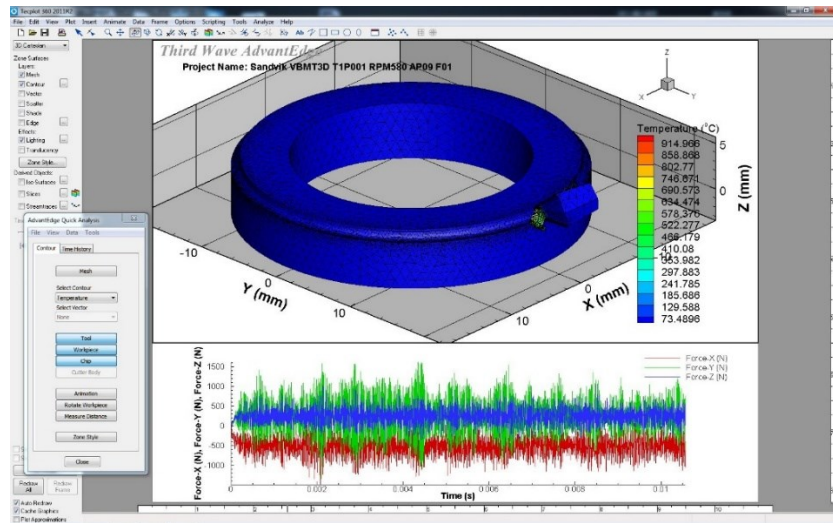
3.8 FEA Simulation by AdvantEdge

For a standard desktop computer with Intel CPU i7-7700K 4.2Ghz 4 cores 8 threads, one FEA simulation of the 3-D turning with high accuracy needs 7 days or more. Therefore, for 3-D FEA simulation by AdvantEdge, one L_9 orthogonal array could be finished with multiple computers in a month. Table 3-10 is the experiment array for FEA simulation. As mentioned before, this experiment array is designed for outer diameter cutting tool#1 VBMT160408 insert. Material is GH4169 with HRC 38 hardness. It's a dry run experiment with no coolant added. The simulation path length is from 0~360 degrees which means cutting one helix circle around.

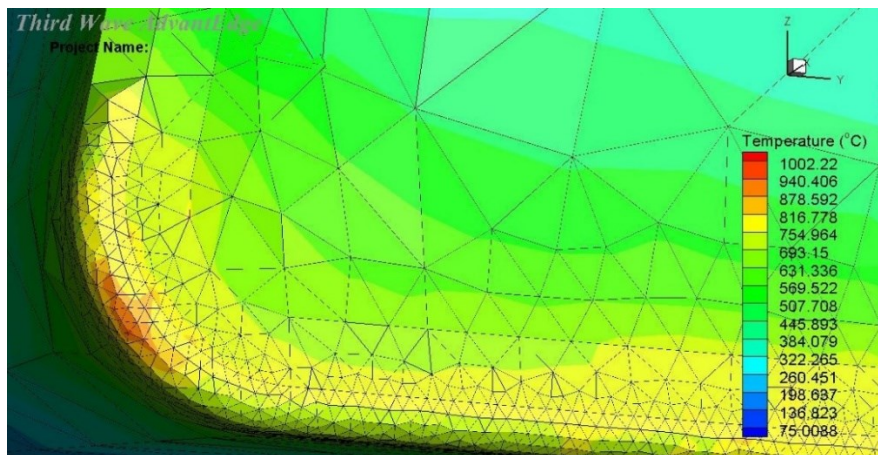
Table 3-10 Experiment array for FEA simulation

Experiment No.	Cutting speed <i>m/min</i>	Depth of cut <i>mm</i>	Feed rate <i>mm/rev</i>	Temperature <i>C°</i>	Force X N	Force Y N	Force Z N
1	56.5	0.9	0.1	773	480	242	241
2	56.5	1.7	0.17	816	966	262	388
3	56.5	2.5	0.25	867	1549	285	570
4	67.8	0.9	0.17	845	559	236	203
5	67.8	1.7	0.25	859	1108	275	398
6	67.8	2.5	0.1	801	1066	246	617
7	79.2	0.9	0.25	855	639	234	177
8	79.2	1.7	0.1	861	819	255	441
9	79.2	2.5	0.17	881	1291	242	559

After computation, all of the simulation results can be found in Telecom360® postprocessor as shown in Figure 3.23(a). All cutting forces are recorded from average value during simulation length. Temperature is chosen from the max value of the cutting edge like Figure 3.23(b) shows. The temperature distribution on cutting edge can be used for predicting the tool wear and the worst location on cutting edge. The chip deformation is shown in Figure 3.24.

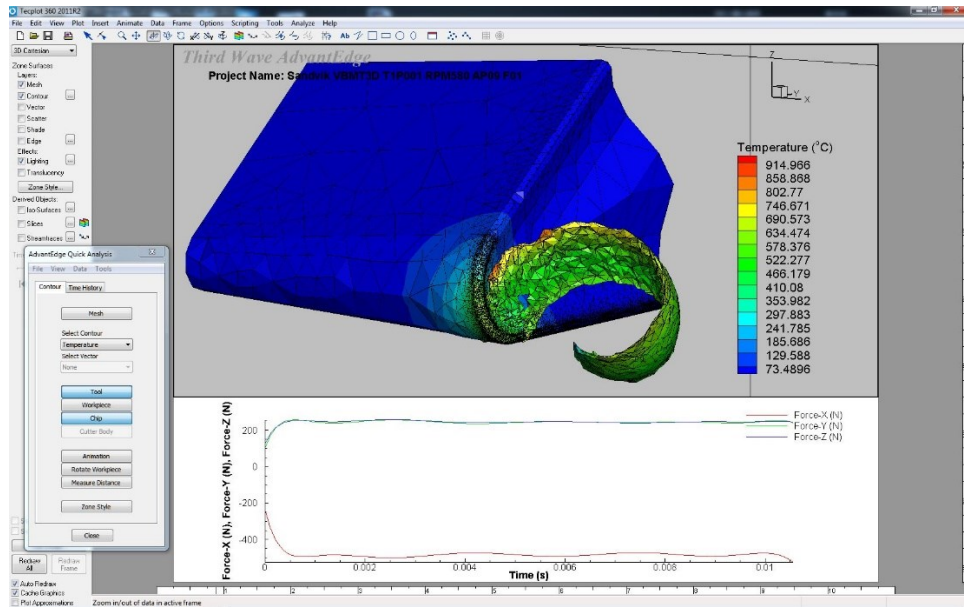


(a)

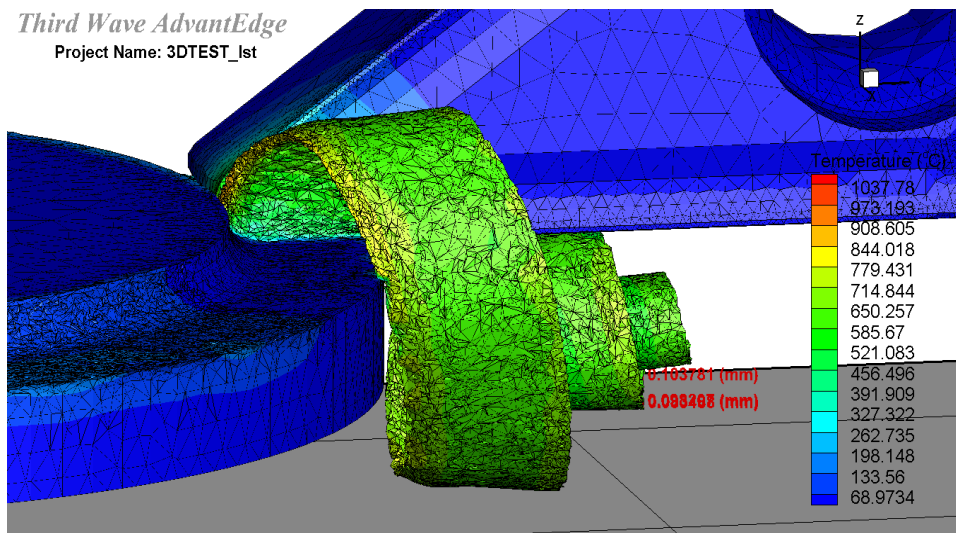


(b)

Figure 3.23 (a) Telecom 360 postprocessor, (b) Cutting edge temperature distribution



(a)

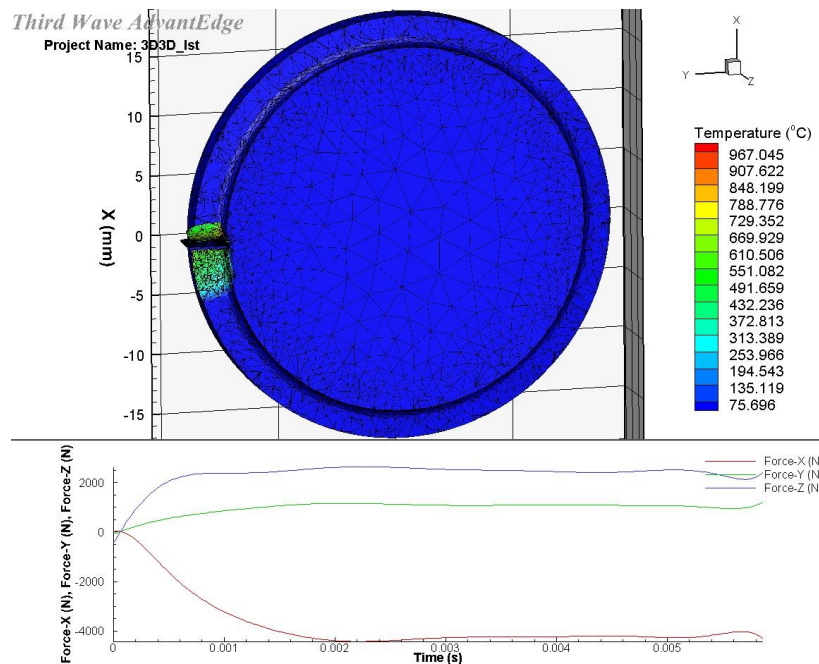


(b)

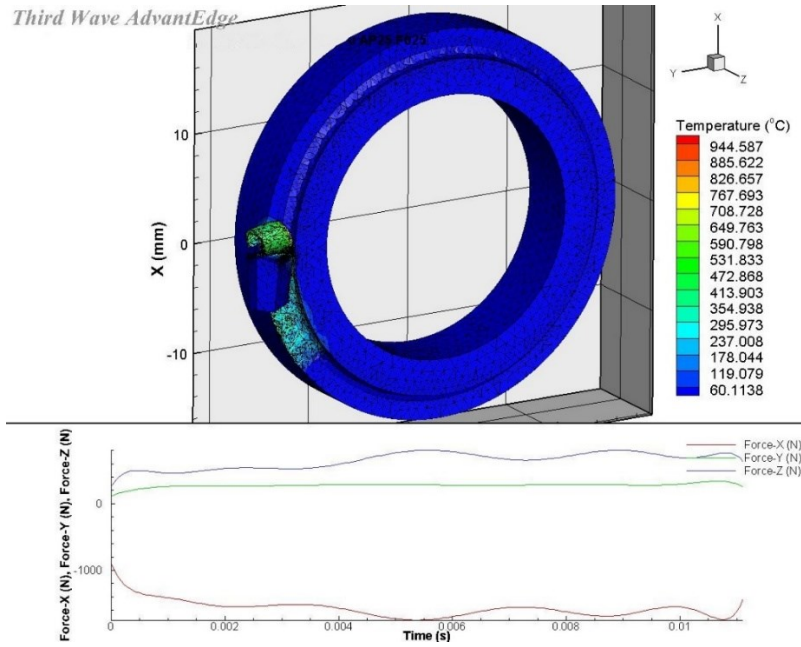
Figure 3.24 (a) Simulation of chip deformation, (b) Chip deformation after one revolution

3.9 Advantages of the Optimal Simulation Method

By using the AdvantEdge simulation with the built-in 3-D model as shown in Figure 3.25(a), the simulation results are obtained. The results are compared with the optimal simulation result as shown in figure 3.25(b). These two tests have the same cutting parameters, which are: feed 0.25mm, depth of cut 2.5mm and cutting speed 56.5m/min. The optimal simulation has accurate 3-D models and optimized mesh settings. As a result, the cutting speed force is reduced by 64% (4416N to 1549N), the radial force is reduced by 75% (1153N to 285N), and the feed force is reduced by 80% (2666N to 570N). From previous cutting experiments [20,33], the cutting speed force is near 1200N, radial force is near 200N, feed force is near 600N. Therefore, by using the optimal simulation method in this thesis, the result is closer to the previous researches.



(a)



(b)

Figure 3.25 (a) Simulation with built-in 3-D model and mesh setting, (b) Simulation with accurate 3-D model and optimized mesh setting

In addition, as Table 3-11 and Figure 3.26 show, by using the optimal simulation method, the meshing time is saved by 90%, and the simulation time is saved by 42%.

Table 3-11 Simulation and meshing time comparison

Method	Meshing time	Simulation time
Optimal simulation method	00 min 43 s	7 days
Built-in simulation method	08 min 09 s	12 days

Name	Current Length	Total Length	Status	Approx. Time Remaining
Optimized	9.7697E-03	360.0	Running	7 Days
3D3D	0.8136	360.0	Running	12 Days

Figure 3.26 Simulation time screenshot from AdvantEdge workbench

CHAPTER 4 CUTTING PARAMETERS OPTIMIZATION

4.1 Introduction of Cutting Parameters Optimization

Nowadays, many optimization approaches are used for cutting parameters optimization such as particle swarm optimization (PSO), artificial bee colony algorithm [23], genetic algorithm (GA) [26], Taguchi method [28] and analysis of variance (ANOVA) [29]. The algorithm based on neural networks and genetic algorithms needs a larger number of samples to train itself in order to meet accuracy. For this study, the samples provided are limited because of the simulation time and computer performance. Therefore, when a turning simulation number is less than 200, the analysis of variance approach is suitable and could save more time on simulation.

4.2 Analysis of S/N Ratio

The signal to noise (S/N) ratio is the basic concept in the Taguchi method. The S/N ratio uses signals to represent the target value for simulation output. And it also uses noise to represent the unwished output. For experimental design results analysis, a larger S/N ratio of specified parameters means that the parameters will have more influence than other parameters with smaller S/N ratio. In this study, the smaller-the-better quality characteristic [28] was used to find the cutting force and optimized temperature value. The equation for smaller-the-better is:

$$\frac{S}{N} = -10 \log \frac{1}{n} \left(\sum_{i=1}^n y^2 \right)$$

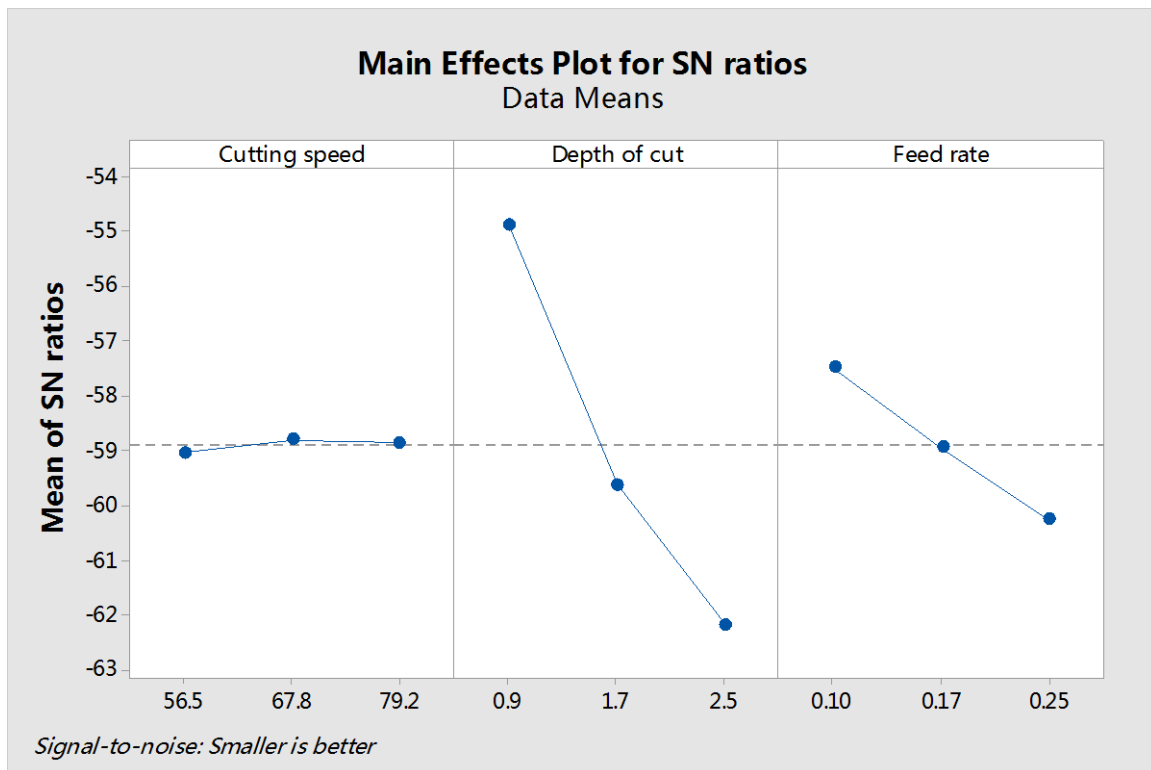
Here n is the number of observations and y is the value of target output. For example,

Table 4-1 and Figure 4.1 show the S/N ratio result to minimize cutting force X on cutting speed direction.

Table 4-1 S/N ratio for minimize force X

Level	Cutting speed	Depth of cut	Feed rate
1	-59.04	-54.89	-57.48
2	-58.80	-59.62	-58.96
3	-58.86	-62.19	-60.27
Max-min	0.24	7.30	2.79
Rank	3	1	2

Figure 4.1 S/N response graph for force X



4.3 Analysis of Variance

The analysis of variance (ANOVA) is used to investigate how cutting parameters affect the rate for simulation and experiment output. The total sum of squared deviations SS can be calculated from total S/N ratio \bar{x} and the S/N ratio for the No. i experiment x_i . This equation is shown below:

$$SS = \sum_{i=1}^n (x_i - \bar{x})^2$$

Total sum of error squared deviations is SS_e . Main square of error MS_e is the ratio of the sum of error squared deviations to degrees of freedom. Main square MS is the ratio of the sum of squared deviations to degrees of freedom. The F test, also called joint hypotheses test, is used to check which parameter has the significant effect on the output. It can be calculated as:

$$F = MS^2 / MS_e^2$$

The F-Value for each parameter is the ratio of the main squared deviations to main squared error. To verify whether it has a significant effect or not, a reference F-table should be used for comparisons. For 0.05 right-tail probabilities (α), the F-table is shown below in Table 4.2.

Table 4-2 F-table for $\alpha=0.05$

DOF1 DOF2	1	2	3	4	5	6	7	8
1	161.4476	199.5000	215.7073	224.5832	230.1619	233.9860	236.7684	238.8827
2	18.5128	19.0000	19.1643	19.2468	19.2964	19.3295	19.3532	19.3710
3	10.1280	9.5521	9.2766	9.1172	9.0135	8.9406	8.8867	8.8452
4	7.7086	6.9443	6.5914	6.3882	6.2561	6.1631	6.0942	6.0410
5	6.6079	5.7861	5.4095	5.1922	5.0503	4.9503	4.8759	4.8183
6	5.9874	5.1433	4.7571	4.5337	4.3874	4.2839	4.2067	4.1468
7	5.5914	4.7374	4.3468	4.1203	3.9715	3.8660	3.7870	3.7257
8	5.3177	4.4590	4.0662	3.8379	3.6875	3.5806	3.5005	3.4381

From Table 3-10, because of each parameter $DOF = 2$, therefore $DOF1$ and $DOF2$ should be 2 and the $F_{0.05} = 19.0$. When cutting parameter F-Value is larger than 19, it will significantly affect output. The larger F-Values represent greater dispersion. The P-Value or probability value is the probability of getting unwished output under specified input. The smaller the P-Value, the larger the influence. Generally speaking, when a P-Value for cutting parameter is less than 0.05, the change of this parameter has a significant effect for simulation output.

Table 4-3 Analysis of variance for force X

Source	DOF	SS	MS	F-Value	P-Value
Cutting speed	2	14380	7190	1.16	0.462
Depth of cut	2	829598	414799	67.20	0.015
Feed rate	2	144507	72253	11.71	0.079
Error	2	12345	6172		
Total	8	1000829			

According to Table 4-3, the main contribution to force X is the depth of cut, then feed rate, and then cutting speed. In order to diminish cutting speed force, the depth of cut should be as small as possible, then it should decrease the feed rate and cutting speed. Based on the cutting parameter range, S/N ratio and ANOVA analyses, the optimal cutting parameters can be found in order to diminish cutting force X. There is the cutting speed of 50m/min, the feed rate at 0.1mm/rev, and the depth of cut at 0.9mm.

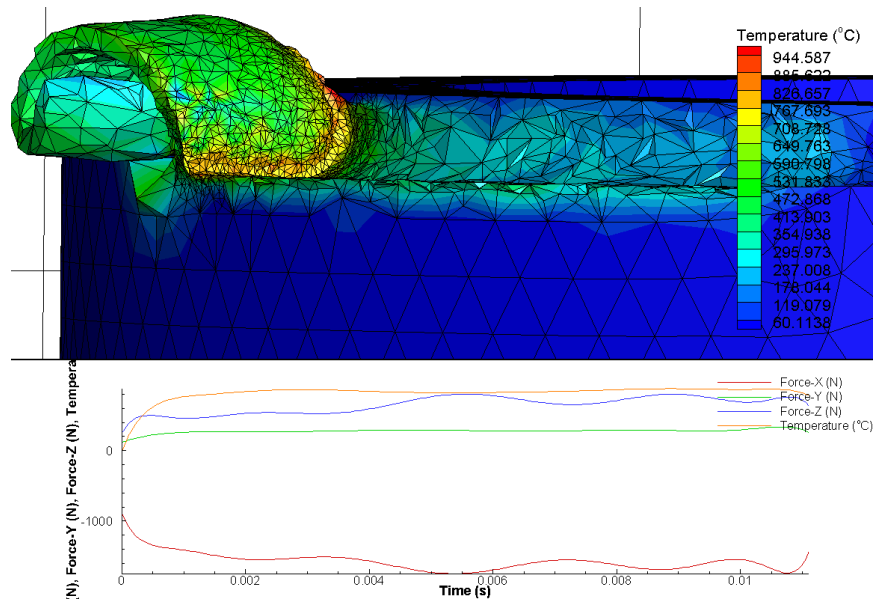
4.3 Verification

After the optimal cutting parameters have been selected, the last step is to use AdvantEdge simulation to predict the performance and to do a real experiment to verify the improvement.

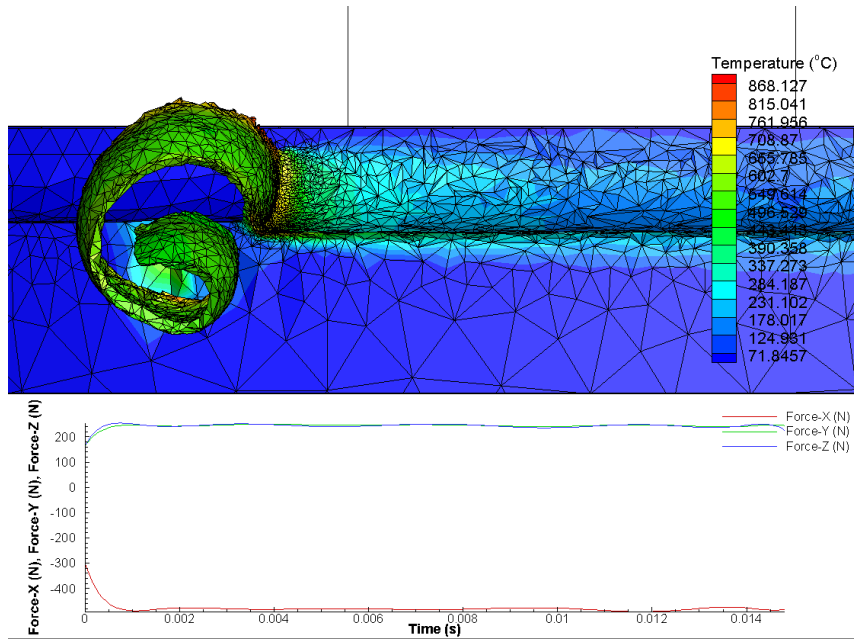
Table 4-4 and Figure 4.2 show the optimized cutting parameters simulation results in AdvantEdge.

Table 4-4 Optimized cutting parameters simulation result

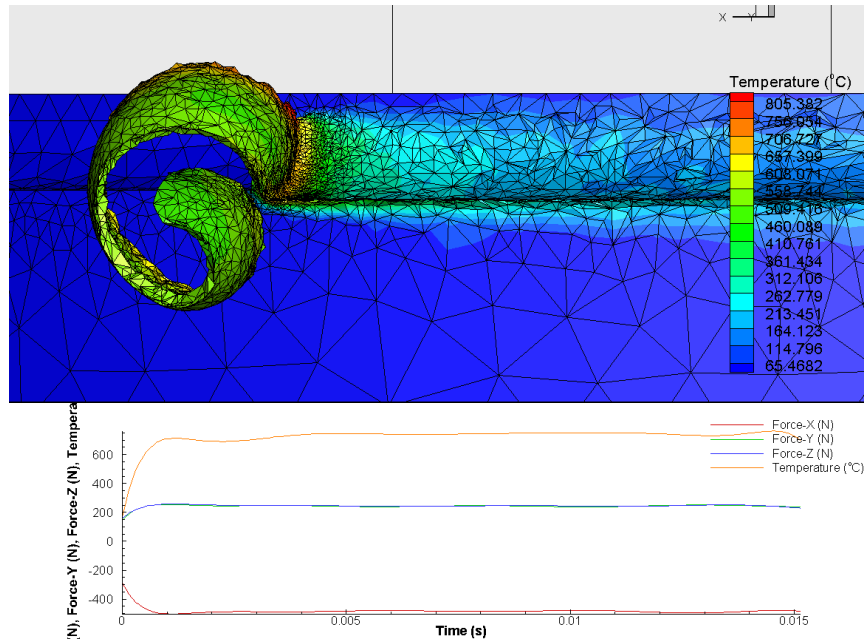
Experiment No.	Cutting speed <i>m/min</i>	Depth of cut <i>mm</i>	Feed rate <i>mm/rev</i>	Temperature <i>C°</i>	Force X <i>N</i>	Force Y <i>N</i>	Force Z <i>N</i>
Optimized	50	0.9	0.1	728	455	236	241
1	56.5	0.9	0.1	773	480	242	241
3	56.5	2.5	0.25	867	1549	285	570



(a)



(b)



(c)

Figure 4.2 (a) No.3 experiment (b)No.1 experiment (c) Optimized experiment

Compared with the worst case in cutting range, the cutting force X changed from 1549N to 455N. Also, it is 25N less than the experiment No.1 in Table 4-4 because the cutting speed decreases. Therefore, the simulation verifies that the cutting parameters are optimized and that they can be used for the decrease of the cutting force X, which is critical for tool life and surface roughness.

CHAPTER 5 CONCLUSIONS AND FUTURE WORK

5.1 Conclusions

In this thesis, in order to present optimized cutting parameters for GH4169 superalloy turning, an accurate approach to design the turning tool and the GH4169 workpiece is proposed. For the modeling of the insert, the rake face and cutting edge are modeled based on profiler measurements and on the ISO standard. For tool holder modeling, the trilinear coordinates measuring instrument has been used for finding the real location of the insert slot plane, which is extremely important for the next FEA simulation. The workpiece modeling for FEA was optimized for saving simulation time. And a detailed workpiece model with chunks was also provided for different toolpaths and tools simulation. The JC constitutive model for GH4169 has been programmed for the user-defined model in AdvantEdge. Compared with default material, a better temperature distribution has been improved in FEA result. For meshing, a sensitive rate test on tool rake face shows the main contribution on FEA accuracy for turning is insert cutting edge. The increase of meshing accuracy on the cutting edge will improve the result precision dramatically but also will increase simulation time.

Also, the Taguchi optimization method has been used to design the orthogonal experimental table, which could save simulation time and give the optimized cutting parameters for GH4169 turning process.

5.2 Future Work

For future research, several topics are considered to expand the present research work.

In order to create the FEA model for whole slender shaft turning, certain factors should be considered, including bending deformation, three-jaw chuck deformation and concentricity. The difference between idea circular ring and actual slender needs to be further discussed for workpiece design.

For optimization, the toolpath needs be optimized after cutting parameters change. The other optimization methods can be used for comparing the optimized results. A real experiment needs to be done for confirmation of FEA accuracy.

Due to the FEA simulation taking a lot of time, a better meshing way needs to be found for time efficiency. More simulation experiments need to be done for different tools with their cutting parameter range.

REFERENCES

1. I.A Choudhury, M.A El-Baradie, Machinability of nickel-base super alloys, Journal of Materials Processing Technology Volume 77, Issues 1–3, 1998, Pages 278-284.
2. F. Taricco, Effect of machining and shot peening on the residual stresses of superalloy turbine discs, ASME 1995 International Gas Turbine and Aeroengine Congress and Exposition Volume 5, 1995, Pages 100-105.
3. A.R.C. Sharman, J.I. Hughes and K. Ridgway, An analysis of the residual stresses generated in Inconel 718TM when turning, Journal of Materials Processing Technology 173, 2006, Pages 359-367.
4. K.J. Weinmann, B.F. Von Turkovich, A hybrid analytical mechanics of tool-workpiece engagement and incipient deformation in machining of 70/30 brass, ASME, 1971, Pages 1079-1089.
5. E. Usui, T. Shirakashi and T. Kitagawa, Analytical prediction of cutting tool wear, Wear 100, 1984, Pages 129-151.
6. J. Dhananjay, Finite element simulation of machining a nickel-based superalloy Inconel 718, Oklahoma State University, 2004.
7. N. Ahmed, A.V. Mitrofanov, V.I. Babitsky and V.V. Silberschmidt, 3D finite element analysis of ultrasonically assisted turning, Computational Materials Science 39, 2007, Pages 149-154
8. R. Li, A.J. Shih, Finite element modeling of 3D turning of titanium, Int J Adv Manuf Technol, 2005.
9. J. Zhou, D. Yip-Hoi and X. Huang, A hybrid analytical solid modeler and feature-based

- methodology for extracting tool-workpiece engagements in turning, ASME Volume 7, 2007, Pages 192-202.
10. R.S. Pawade, S.S. Joshi, P.K. Brahmanekar and M. Rahmanc, An investigation of cutting forces and surface damage in high-speed turning of Inconel 718, Journal of Materials Processing Technology Volumes 192–193, 2007, Pages 139–146.
 11. E. Uhlmann, Finite Element Modeling and Cutting Simulation of Inconel 718, Annals of the CIRP Volume 56, 2007.
 12. T. Ozel, I. Llanos, 3D finite element modeling of chip formation process for machining Inconel 718: comparison of FE software predictions, Machining Science and Technology Volume 15, 2011, Pages 21-46.
 13. F. Jafarian, M.I. Ciaran, D. Umbrello, Finite element simulation of machining Inconel 718 alloy including microstructure changes, International Journal of Mechanical Sciences Volume 88, 2014, Pages 110-121.
 14. A.V. Mitrofanov, V.I. Babitsky, V.V. Silberschmidt, Finite element analysis of ultrasonically assisted turning of Inconel 718, Journal of Materials Processing Technology Volumes 153–154, 2004, Pages 233-239.
 15. R.K. Yadav, K. Abhishek, S.S. Mahapatra, A simulation approach for estimating flank wear and material removal rate in turning of Inconel 718, Simulation Modeling Practice and Theory 52, 2015, Pages 1-14.
 16. D. Zhang, X.M. Zhang and H. Ding, Hybrid digital image correlation–finite element modeling approach for modeling of orthogonal cutting process, ASME Volume 140, 2018.
 17. L. Tang, R.G. Landers, S.N. Balakrishnan, Parallel turning process parameter optimization

- based on a novel heuristic approach, *Journal of Manufacturing Science and Engineering* Volume 130, 2008.
18. I. Al-Zkeri, J. Rech, T. Altan, H. Hamdi and F. Valiorgue, Optimization of the cutting edge geometry of coated carbide tools in dry turning of steels using a finite element analysis, *Machining Science and Technology* Volume 13, 2009.
 19. K. Chomsamutr, S. Jongprasithporn, The cutting parameters design for product quality improvement in turning operations: Optimization and validation with Taguchi method, *The 40th International Conference on Computers & Industrial Engineering*, 2010.
 20. A. Del Prete, A.A. De Vitis, L. Filice, S. Caruso and D. Umbrello, Tool engage investigation in nickel superalloy turning operations, *Key Engineering Materials* Volumes 504-506, 2012.
 21. S. Zhang, J.F. Li, Y.W. Wang, Tool life and cutting forces in end milling Inconel 718 under dry and minimum, *Journal of Cleaner Production* Volume 32, 2012, Pages 81-87.
 22. C. Camposeco-Negrete, J. Calderón-Nájera, J. C. Miranda-Valenzuela, Optimization of cutting parameters in turning of AISI 1018 steel with constant material removal rate using robust design for minimizing cutting power, *ASME 2013 International Mechanical Engineering Congress and Exposition* Volume 2B, 2013.
 23. A.R. Yildiz, Optimization of cutting parameters in multi-pass turning using artificial bee colony-based approach, *Information Sciences* Volume 220, 2013, Pages 399-407.
 24. S. Vijay, V. Krishnaraj, Machining parameters optimization in end milling of Ti-Al-4V, *Procedia Engineering* Volume 64, 2017, Pages 1079-1088.
 25. Z.H. Wang, J.T. Yuan, Z.B. Yin and C. Li, Study on high-speed cutting parameters optimization of AlMn1Cu based on neural network and genetic algorithm, *Advances in Mechanical*

- Engineering Volume 8, 2016, Pages 1783–1792.
26. B. Satyanarayana, M.D. Reddy, P.R. Nitin, Optimization of controllable turning parameters for high speed dry machining of super alloy: FEA and experimentation, *Materials Today: Proceedings* Volume 4, 2017, Pages 2203-2212.
 27. L.L. Li, C.B. Li, Y. Tang and L. Li, Integration of process planning and cutting parameter optimization for energy-aware CNC machining, 2017 13th IEEE Conference on Automation Science and Engineering (CASE), 2017.
 28. G. Taguchi, S. Chowdhury, S. Taguchi, *Robust Engineering*, McGraw-Hill, 2000.
 29. W.H. Yang, Y.S. Tarng, Design optimization of cutting parameters for turning operations based on the Taguchi method, *Journal of Materials Processing Technology* Volume 84, 1998, Pages 122-129.
 30. International organization for standardization, ISO 5610: Tool holders with rectangular shank for indexable inserts, 2014.
 31. International organization for standardization, ISO 3364: Indexable hardmetal (carbide) inserts with rounded corners, with cylindrical fixing hole – Dimensions, 2011.
 32. Third wave systems, *AdvantEdge 7.1 user's manual*, 2015.
 33. K. Jemielniak, Rough turning of Inconel 718, *Advances in Manufacturing Science and Technology* Volume 33, 2009.